



1 **Assessing acetone for the GISS ModelE2.1 Earth system model**

2 Alexandra Rivera¹, Kostas Tsigaridis^{2,3}, Gregory Faluvegi^{2,3}, Drew Shindell⁴

3 ¹Pratt School of Engineering, Duke University, Durham, NC, 27708, USA

4 ²Center for Climate Systems Research, Columbia University, 2880 Broadway, New York, NY, 10025, USA

5 ³NASA Goddard Institute for Space Studies, 2880 Broadway, New York, NY, 10025, USA

6 ⁴Nicholas School of the Environment, Duke University, Durham, NC, 27708, USA

7 *Correspondence to:* Kostas Tsigaridis (kostas.tsigaridis@columbia.edu)

8 **Abstract.** Acetone is an abundant volatile organic compound in the atmosphere with important influence on ozone and oxidation
9 capacity. Direct sources include anthropogenic, terrestrial vegetation, oceanic, and biomass burning emissions. Acetone is also
10 produced chemically from other volatile organic compounds. Sinks include deposition onto the land and ocean surfaces, as well as
11 chemical loss. Acetone's lifetime is long enough to allow transport and reactions with other compounds remote from its sources.
12 The latest NASA Goddard Institute for Space Studies (GISS) Earth System Model, ModelE2.1, simulates a variety of Earth system
13 interactions. Previously, acetone had a very simplistic representation in the ModelE chemical scheme. This study assesses a more
14 sophisticated acetone scheme, in which acetone is a full 3-dimensional tracer, with explicit sources, sinks and atmospheric
15 transport. We evaluate the new global acetone budget in the context of past literature. Anthropogenic emissions, vegetation
16 emissions, biomass burning, and deposition representations agree well with previous studies. Chemistry and the ocean contribute
17 to both sources and sinks of acetone, with their net values agreeing with the literature, although their individual source and sink
18 terms appear to be overestimated for chemistry and underestimated for ocean fluxes. We find the production of acetone from
19 precursor hydrocarbon oxidation has strong leverage on the overall chemical source, indicating the importance of accurate molar
20 yields for this source. Spatial distributions reveal that ocean uptake of acetone is strongest in northern latitudes, while production
21 is mainly in mid-southern latitudes. The seasonality of acetone-related processes was also studied in conjunction with field
22 measurements around the world. These comparisons show promising agreement, but have shortcomings at urban locations, since
23 the model's resolution is too coarse to capture behavior in high-emission areas. Overall, our analysis of the acetone budget aids
24 the development of this tracer in the GISS ModelE2.1, a crucial step to understanding the role of acetone in the atmosphere.

25 **1 Introduction**

26 Acetone (C₃H₆O) is an abundant oxygenated volatile organic compound (VOC) that has important connections to ozone and the
27 atmosphere's self-cleansing oxidation capacity (Read et al., 2012). Acetone's dynamic presence in Earth's atmosphere can be
28 described through sources, sinks, and mechanisms of transport. Extensive literature has discussed the nature of these sources and
29 sinks, and some are more well-constrained than others.

30

31 Primary sources of acetone in the atmosphere include anthropogenic, terrestrial vegetation, and biomass burning emissions. Past
32 literature has found the fluxes of these sources to range between 1-2 Tg yr⁻¹, 30-45 Tg yr⁻¹, 2.5-4.5 Tg yr⁻¹, respectively (Beale et
33 al., 2013; Brewer et al., 2017; Elias et al., 2011; Fischer et al., 2012; Folberth et al., 2006; Jacob et al., 2002; Singh et al., 2000;
34 Wang et al., 2020). Chemical production from other VOCs with 3 or more carbon atoms, each with their own molar yields, is
35 another source of acetone in the atmosphere (Brewer et al., 2017; Fischbeck et al., 2017; Hu et al., 2013; Jacob et al., 2002; Singh
36 et al., 2000; Weimer et al., 2017).



37

38 Sinks of acetone include wet and dry deposition onto the land surface, as well as chemical loss. Wet deposition occurs within and
39 below clouds, due to the high solubility of acetone, which depends on its Henry's Law coefficient (Benkelberg et al., 1995). Dry
40 deposition occurs on the land surface. Chemical loss of acetone forms radicals, either through oxidation by OH or photolysis. Past
41 literature has estimated the acetone sinks to be 10-30% dry deposition, and 40-85% chemical loss (Arnold et al., 2005; Elias et al.,
42 2011; Fischer et al., 2012; Khan et al., 2015; Singh et al., 1994). The estimated fluxes are 10-16 Tg yr⁻¹ and 45-60 Tg yr⁻¹ for total
43 deposition and chemical loss, respectively (Arnold et al., 2005; Brewer et al., 2017; Dufour et al., 2016; Elias et al., 2011; Fischer
44 et al., 2012; Jacob et al., 2002; Khan et al., 2015; Marandino et al., 2005; Singh et al., 2000; Wang et al., 2020).

45

46 The ocean surface is a bidirectional flux that provides both a source and a sink for acetone. Ocean surface conditions such as wind
47 speed, sea surface temperature, and seawater concentration of acetone can influence the direction and magnitude of ocean-acetone
48 exchange (Wang et al., 2020). Previous literature estimates an oceanic source flux of 25–50 Tg yr⁻¹ and oceanic uptake flux of
49 35–60 Tg yr⁻¹. However, there is little consensus in the literature on whether the ocean serves as a net source or sink of acetone,
50 with some studies indicating a net oceanic source (Beale et al., 2013; Jacob et al., 2002; Wang et al., 2020), and other studies
51 indicating a net oceanic sink (Brewer et al., 2017; Elias et al., 2011; Fischer et al., 2012; Wang et al., 2020).

52

53 In addition to a global annual mean atmospheric budget, previous studies have reported the seasonality of acetone-related processes.
54 Past studies have compared monthly estimates of acetone mixing ratios to field measurements of European sites from Solberg et
55 al. (1996) (Arnold et al., 2005; Elias et al., 2011; Jacob et al., 2002). Comparisons with these European sites have emphasized the
56 seasonal variability of acetone emissions, as nearly all sites portray a summer maximum and winter minimum of acetone
57 abundance. Vegetation emissions from June to September, along with chemical sources, have an especially strong contribution to
58 this seasonality. The winter minimum of acetone is aided by an ocean sink at coastal sites (Jacob et al., 2002).

59

60 Other studies have described spatial distributions and seasonal dependence of ocean fluxes of acetone (Fischer et al., 2012; Wang
61 et al., 2020). A model by Fischer et al. (2012) proposed a net ocean sink of 2 Tg yr⁻¹, characterized ocean uptake of acetone as
62 strongest in northern latitudes year-round, and strongest in the high southern latitudes during the winter. An oceanic acetone source
63 was dominant in the tropical regions, with an exception off the Western coasts of Central America and Central Africa (Fischer et
64 al., 2012). A model by Wang et al. (2020) that varied surface seawater acetone concentration through a machine learning approach
65 also proposed a net ocean sink year-round. This net sink was strongest in December-February, and weakest in March-May.

66

67 The vertical distribution of acetone has been modelled between the seasons of May-October and November-April in the surface
68 and troposphere (Fischer et al., 2012). Acetone concentrations are generally higher in the lower altitudes due to proximity to surface
69 emissions. Surface-level acetone has been measured over a variety of terrestrial and oceanic sites around the world (de Gouw et
70 al., 2004; Dolgorouky et al., 2012; Galbally et al., 2007; Guérette et al., 2019; Hu et al., 2013; Huang et al., 2020; Langford et al.,
71 2010; Lewis et al., 2005; Li et al., 2019; Read et al., 2012; Schade & Goldstein, 2006; Singh et al., 2003; Solberg et al., 1996;
72 Warneke & de Gouw, 2001; Yoshino et al., 2012; Yuan et al., 2013), and in some cases, these measurements were taken over a
73 variety of months to provide a sense of seasonality (Dolgorouky et al., 2012; Hu et al., 2013; Read et al., 2012; Schade & Goldstein,
74 2006; Solberg et al., 1996). Additionally, vertical distributions of acetone have been measured through NASA's Atmospheric
75 Tomography Mission (ATom) campaigns (Thompson et al., 2022). The ATom-1, ATom-2, ATom-3, and ATom-4 campaigns took
76 place during July-August 2016, January-February 2017, September-October 2017, and April-May 2018, respectively. Each



77 campaign provided mixing ratios for a variety of VOCs in profiles from the marine boundary layer up to the upper
78 troposphere/lower stratosphere (Apel et al., 2021).

79

80 The NASA Goddard Institute for Space Studies (GISS) ModelE2.1 Earth System Model (Kelley et al., 2020) has the capability of
81 simulating a variety of Earth system interactions, is used both to interpret and predict past and future climate, and routinely
82 participates in the Climate Model Intercomparison Projects (CMIP) and Intergovernmental Panel for Climate Change (IPCC)
83 reports. Here we used this model and enhanced it by adding acetone as an independent chemical tracer (Kelley et al., 2020).
84 Previously, acetone had a very simplistic representation in the model's chemical scheme (Shindell et al., 2003), in which acetone's
85 spatial variation was parameterized based on the difference of the model's zonal mean distribution of isoprene and that tracer's
86 three-dimensional distribution. Acetone's lifetime is long enough to be transported remote from sources, but not long enough to
87 become uniformly mixed, and therefore its simulated distribution should benefit from a more realistic implementation. We
88 developed a greatly improved acetone tracer scheme by making prognostic calculations of the 3-dimensional distribution of acetone
89 as a function of time. We evaluated its atmospheric burden and lifetime as well as source/sink fluxes (anthropogenic emissions,
90 vegetation emissions, biomass burning, deposition, ocean, and chemistry) against other models and its concentration against field
91 measurements. This work aims to provide a holistic assessment of the abundance of acetone in the atmosphere.

92 **2 Methodology**

93 Our 'Baseline' simulation is a climatological mean with year 2000 conditions, chosen to be relatively modern without precluding
94 comparison with models in older literature. The 1996-2004 mean of prescribed emissions from Hoesly et al. (2018) were used,
95 along with the 1996-2005 mean sea surface temperature and sea ice cover as described in Kelley et al., (2020). An additional
96 simulation, 'Nudged_ATom', was conducted to compare more directly with ATom field measurements. This simulation employed
97 nudged winds (from MERRA2) (Gelaro et al., 2017) and ocean surface conditions and trace gas and aerosol emissions changing
98 with time during 2016-2018.

99 **2.1 Sources**

100 **2.1.1 Anthropogenic emissions**

101 Anthropogenic emissions were prescribed using the 1996-2004 averages of the Community Emissions Data System (CEDS)
102 emissions from Hoesly et al. (2018) as prepared for the GISS contributions to the Coupled Model Intercomparison Project, Phase
103 6 (CMIP6) (Kelley et al., 2020). These include sources from agriculture, the energy sector, the industrial sector,
104 residential/commercial/other, international shipping, solvents production and application, the transportation sector, and waste. In
105 line with past studies, we base acetone emissions on that of ketones. VOC23-ketones emissions from Hoesly were scaled down by
106 a ratio of acetone molecular weight to an average ketone molecular weight ($58.08 \text{ g mol}^{-1}/75.3 \text{ g mol}^{-1}$). Maintaining the resulting
107 spatial and temporal pattern of emissions, the magnitudes were then tuned to be close to that of Fischer et al., (2012), resulting in
108 a total of about 1 Tg yr^{-1} . This resulted in roughly 36.5% of CEDS VOC23-ketones used as acetone emissions. Lacking an accurate
109 way to obtain acetone aircraft emissions from the bulk VOCs available in the emission inventory, we have neglected that sector in
110 the simulations.



111 2.1.2 Terrestrial vegetation emissions

112 Emissions from land vegetation were derived from the Model Emissions of Gases and Aerosols from Nature (MEGAN), version
113 2.1 (Guenther et al., 2012), a new contribution to the ModelE. Emission response algorithms in the MEGAN2.1 model are derived
114 from input leaf area indices, solar radiation, temperature, moisture, CO₂ concentrations, and plant functional types and composition
115 of species (Guenther et al., 2012). The acetone vegetation emissions in the Baseline simulation in GISS ModelE2.1 are calculated
116 to equal 36.1 Tg yr⁻¹.

117 2.1.3 Biomass burning emissions

118 Acetone emissions were prescribed from a 1996-2004 average of the NMVOC-C3H6 species from version 2.1 of the biomass
119 burning dataset of van Marle et al. (2017), used by CMIP6. The acetone mass flux from biomass burning in the Baseline simulation
120 was 1.59 Tg yr⁻¹.

121

122 Figure 1 shows the biomass burning emission rate chosen for this study, and how it lies within the range of substantial interannual
123 variability. During the 20-year period shown, emissions averaged 1.463 Tg yr⁻¹, with a standard deviation of 0.402, and a spike in
124 the earlier years of emissions over 2.75 Tg yr⁻¹ is also observed (Figure 1). On top of any differences across emission inventories,
125 the years considered when reporting emissions may be the reason for variability between models (e.g. 2.40 – 2.80 Tg yr⁻¹ from the
126 2006 GFED-v2 emission inventory in Elias et al. (2011) and Fischer et al. (2012), compared to 3.22 Tg yr⁻¹ from 1997-2001 in
127 Folberth et al. (2006)).

128 2.2 Sinks

129 2.2.1 Deposition

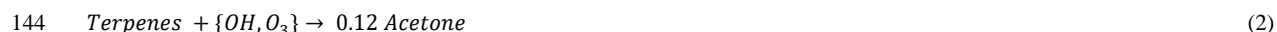
130 Both dry and wet deposition of acetone were included in the model, although dry deposition was, on average, 91% of total
131 deposition. The wet deposition scheme is given by Koch et al., (1999). Acetone and other species are transported within and below
132 clouds, and soluble gases are deposited depending on the conditions of the grid box they are in and a Henry's Law Coefficient
133 (Shindell et al., 2001). The Henry's Law Coefficient for acetone used in the GISS ModelE2.1 is 27 mol L⁻¹ atm⁻¹, with a Henry
134 temperature dependence of acetone of 5300 J mol⁻¹ (Benkelberg et al., 1995; Zhou & Mopper, 1990). The dry deposition scheme
135 uses resistance-in-series calculations, global seasonal vegetation data (Chin et al., 1996; Shindell et al., 2001; Wesely & Hicks,
136 1977), and a reactivity factor of $f_0=0.1$. This resulted in an acetone deposition rate in the Baseline simulation of 22.2 Tg yr⁻¹.

137 2.3 Chemistry

138 The GISS ModelE2.1 Baseline simulation estimates a net chemistry change of -20.6 Tg yr⁻¹. The components can be broken up
139 into sources and sinks as follows.

140 2.3.1 Chemical sources

141 The Baseline simulation estimates chemical production to be 33.3 Tg yr⁻¹. The acetone chemical scheme includes two production
142 reactions:



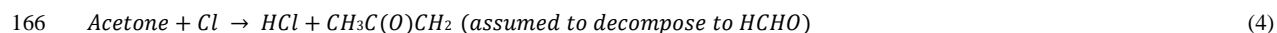
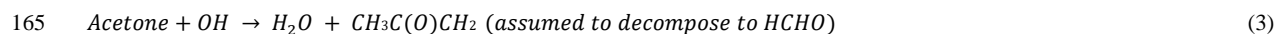


145 In the first reaction, acetone is produced by paraffin, a proxy tracer for paraffinic (saturated) carbon, and OH (Eq. 1). The molar
146 yield of acetone from paraffin was found to be a strong leverage to the overall chemical source (see Section 3.5). A rate coefficient
147 of $8.1\text{E-}13\text{ cm}^3\text{ molecule}^{-1}\text{ s}^{-1}$ was used (Shindell et al., 2003). Previous literature has suggested an acetone yield on a molecular
148 scale of 0.72 (Fischbeck et al., 2017; Jacob et al., 2002; Weimer et al., 2017). Initial tests using a yield of 0.72 resulted in an
149 overestimated chemistry source, leading us to re-evaluate this yield for the specific mixture of VOCs represented in the GISS
150 ModelE2.1. Estimated mole fractions of propane (11%), butane (22%) and pentane (21%) in anthropogenic emissions were
151 multiplied by each compound's acetone molar yield (0.73, 0.95, 0.63, respectively), determining that 42% of paraffin from
152 anthropogenic sources becomes acetone. Estimated mole fractions of propane (9%) and higher alkanes (23%) in biomass burning
153 emissions were multiplied by each compound's acetone molar yield, determining that 25% of paraffin from biomass burning
154 sources becomes acetone. The molar yields used in these calculations were derived with suggestions from the literature (Fischbeck
155 et al., 2017; Jacob et al., 2002; Weimer et al., 2017). An average of the 42% anthropogenic paraffin and 25% biomass burning
156 paraffin was used to conclude that approximately 35% of paraffin from emissions becomes acetone, leading to the molar yield of
157 0.35 in Eq. (1).

158 Additionally, reactions between terpenes and {OH, O₃} were implemented with an acetone yield of 0.12 (Hu et al., 2013; Jacob et
159 al., 2002) (Eq. 2). The rates for these reactions are $2.51\text{E-}11*\exp(444/T)\text{ cm}^3\text{ molecule}^{-1}\text{ s}^{-1}$ for the OH reaction and $1.40\text{E-}14*\exp(-$
160 $732/T)\text{ cm}^3\text{ molecule}^{-1}\text{ s}^{-1}$ for the O₃ reaction, and these coefficients are enhanced from the standard α -pinene one to consider the
161 reactivity variability across mono- and higher terpenes (Tsigaridis and Kanakidou, 2003).

162 2.3.2 Chemical sinks

163 The chemical sink of acetone in the Baseline simulation is estimated to be 53.8 Tg yr^{-1} . The sinks of acetone include oxidation by
164 OH and Cl radicals, and photolysis:



169 The first and second acetone destruction reactions above have rates of $1.33\text{E-}13 + 3.82\text{E-}11*\exp(-2000/T)\text{ cm}^3\text{ molecule}^{-1}\text{ s}^{-1}$ and
170 $7.70\text{E-}11*\exp(-1000/T)\text{ cm}^3\text{ molecule}^{-1}\text{ s}^{-1}$, respectively (Sander et al., 2011) (Eq. 3, 4). Previously, acetone photolysis (which only
171 affected production of radicals and not acetone itself) did not utilize the model's photolysis scheme but was parameterized solely
172 as a function of orbital geometry and atmospheric pressure. In the model updates, photolysis now consists of two separate reactions,
173 where acetone forms either CH₃CO + CH₃ radicals or two CH₃ radicals and CO (Eq. 5, 6). Reaction 5 is pressure-dependent, while
174 reaction 6 is temperature-dependent.

175 2.4 Ocean

176 Bidirectional fluxes of acetone are calculated over ocean based on the "two-phase" model of molecular gas exchange at the air-sea
177 interface of Liss & Slater (1974), as it is described in Johnson (2010). The fluxes are a function of simulated surface temperature
178 and near-surface wind speed but independent of salinity. Henry's Law constants and temperature dependence of solubility for
179 acetone are from Sander (1999). The atmospheric source from ocean water and sink from the atmosphere are calculated assuming
180 a constant concentration of acetone in water (of 15 nM), the lower boundary layer atmospheric concentration, and the total transfer



181 velocity (a combination of water-side and air-side transfer velocities). The GISS ModelE2.1 Baseline simulation calculates the
182 ocean to be a net source of acetone, producing 3.94 Tg yr⁻¹.

183 2.5 Sensitivity studies

184 Sensitivity studies were conducted to determine the influence of key parameters on the acetone budget and its global distribution
185 (Table 1). Specifically, we were interested in seeing how much leverage a given parameter afforded the model by way of an
186 artificial perturbation. Sensitivity studies for chemistry modify the sources of acetone. The Chem_Cl0 and Chem_Terp0
187 simulations provide no formation of acetone from chlorine or terpenes, respectively (Table 1). The importance of paraffin is
188 explored by halving its yield of acetone to 17.5% in the Chem_Par0.5 simulation, and by doubling its yield of acetone to 70% in
189 the Chem_Par2.0 simulation (Table 1). As vegetation was the most prominent source, the Veg_0.7 simulation observes its
190 reduction by decreasing the MEGAN production of acetone by 30% (Table 1). The Ocn_2.0 simulation aims to explore the impact
191 of ocean acetone concentration by doubling it from 15 nM to 30 nM globally (Table 1). The Dep_f0 simulation tested dropping
192 the reactivity factor for dry deposition from 0.1 to zero. Finally, given the high interannual variability of biomass burning emissions,
193 the BB_2.0 simulation explores the impact of doubling those emissions (Table 1).

194 3 Results and model evaluation

195 3.1 Global acetone budget and burden

196 A global acetone budget table was compiled from past global modeling studies to place our estimates in context (Table 2) (Arnold
197 et al., 2005; Beale et al., 2013; Brewer et al., 2017; Dufour et al., 2016; Elias et al., 2011; Fischer et al., 2012; Folberth et al., 2006;
198 Guenther et al., 2012; Jacob et al., 2002; Khan et al., 2015; Marandino et al., 2005; Singh et al., 2000; Singh et al., 2004; Wang et
199 al., 2020). The values of the individual fluxes in our model (global deposition, biomass burning, anthropogenic emissions,
200 vegetation emissions, ocean net/source/sink, and chemistry net/source/sink) were mentioned previously.

201
202 Atmospheric burden describes the total amount of acetone that is in the atmosphere. The GISS ModelE2.1 Baseline simulation
203 estimates the burden to be 2.93 Tg yr⁻¹. Additionally, chemical lifetime and atmospheric lifetime can be derived from burden. The
204 chemical lifetime of acetone is calculated as the burden divided by the chemical sink, whereas total lifetime is the burden divided
205 by all sinks. The chemical and total atmospheric lifetimes for the Baseline simulation are calculated to be 19.9 and 12.3 days,
206 respectively. These values are also placed in the context of previous literature in Table 1.

207
208 The GISS ModelE2.1 Baseline acetone budget is further compared to previous model studies in Figure 2. The calculated fluxes in
209 our Baseline simulation that are less than one standard deviation away from the literature mean include anthropogenic and
210 vegetation emissions, net ocean, net chemistry, chemical production, and chemical destruction (Figure S1). Biomass burning in
211 GISS ModelE2.1 appears as an outlier when compared against 9 previous model studies but can be attributed to the high interannual
212 variability with emissions (as discussed in Section 2.1.3). The value of acetone deposition is on the high (more negative) end in
213 GISS ModelE2.1 relative to 11 previous studies. This might be partially attributed to differences in deposition parametrization
214 across models, as explored by our sensitivity study on dry deposition presented in section 3.5.2. The values for oceanic acetone
215 sources and losses are smaller (in absolute values) than the mean from 7 previous model studies. Nevertheless, the net ocean flux
216 matches the literature well. Lastly, the total atmospheric burden and lifetime calculated by GISS ModelE2.1 are lower than the
217 previous papers, an expected consequence of the higher removal by deposition. The chemical lifetime is also calculated to be at



218 the low end of published literature. As the burden is a function of many different atmospheric parameters, however, it was not the
219 goal to corroborate our estimates with the literature as much as it was for each of the fluxes.

220 **3.2 Spatial distribution of acetone**

221 The global distribution of acetone at the surface is given in Figure 3. It is evident that acetone mixing ratios are largest over the
222 continents, where anthropogenic, vegetation, and other terrestrial sources are located. Over the ocean, acetone mixing ratios are
223 highest downwind of central America and central Africa. A comparison of the GISS ModelE2.1 results against twenty-six prior
224 field measurements shows an overall great agreement, with a root mean squared error of 0.3494 and an R^2 value of 0.8306. To put
225 these results into the context of model evaluation, a similar comparison to field measurements was done for the model's previous
226 acetone scheme. The prior parameterization was designed as a rough representation of acetone oxidized from isoprene in the upper
227 troposphere, without regard for realism near the surface, and this is evident from the comparison with surface observations: a root
228 mean squared error and R^2 value of 1.3620 and 0.0413, respectively. The improvement of the new acetone tracer model in the
229 GISS ModelE2.1 is evident from these statistics.

230

231 A breakdown of the acetone bidirectional fluxes indicates that its chemical production is concentrated over the continents, while
232 chemical destruction is primarily over the oceans (Figure 4). Hotspots of production over the continents include the Southern and
233 Eastern United States and central South America, East and Northern Asia, and Central Africa. Chemical sinks over the oceans are
234 stronger in the tropics than in the high southern or northern latitudes. Annually, there is a net negative flux of about $-20.46 \text{ Tg yr}^{-1}$
235 (Figure 4). Observing the chemical flux over all four seasons, the net loss appears unaffected while the net source changes more
236 significantly, following the seasonality of precursor compounds like isoprene and terpenes (Figure 5). Chemical production is
237 strongest in the months of June/July/August, primarily in the US and Northern Asia. Production is weakest in the months of
238 December/January/February, losing almost all production in the US and Northern Asia entirely. Still, a net negative flux is present
239 for all four seasons (Figure 5).

240

241 The ocean acetone sources and sinks are unevenly distributed across latitudes. Oceanic uptake of acetone is mostly concentrated
242 in the northern rather than the southern oceans, while the ocean acetone source is strongest in the tropics and decreases at higher
243 latitudes of both hemispheres (Figure 6). Combining these two unidirectional fluxes results in the ocean serving as a sink in the
244 northern high latitudes, a source in the tropical latitudes, and near neutral at the high southern latitudes (Figure 7). This finding
245 corroborates very well with findings from Fischer et al. (2012) and Wang et al. (2020). Oceanic bidirectional acetone fluxes present
246 trends over the four seasons (Figure S2). Overall, every season has a positive global mean net flux. However, production becomes
247 strongest in the months of December through May, and weakest in the months of June through November. Off the coast of western
248 South America, the ocean appears to be a net sink of acetone, even though this latitude band is generally a source of acetone. This
249 is especially evident in the months of June/July/August and September/October/November. As the model simulates this location
250 to have high levels of acetone at the surface (Figure 3), we believe the acetone in the air is driving the ocean to be a sink there
251 (Figure S2).

252 **3.3 Vertical distribution of acetone**

253 The vertical distribution of acetone varies by latitude, with near-surface air mixing ratios being higher in the tropics and in the
254 northern midlatitudes. Acetone levels in the atmosphere decrease with height, a direct result of sinks dominating the sources (Figure
255 8). Prior to the implementation of an acetone tracer in the GISS ModelE2.1, when acetone was derived from the zonal mean of



256 isoprene, the vertical distribution looked very different (Figure S3). Acetone was only concentrated around the tropics and did not
257 extend nearly as high into the atmosphere. The complexity of Figure 8 supports the new acetone tracer scheme as a significant
258 improvement to the GISS ModelE.

259

260 Another modelled vertical distribution of acetone, including a differentiation between two long seasons, is explored in Figure 9.
261 In general, it was found that acetone mixing ratios are higher in the months of May-October than in November-April, and that this
262 relationship is stronger in the lower atmosphere (0-2 km) than the upper atmosphere (6-10 km). This finding corroborated well
263 with a similar analysis done by Fischer et al. (2012).

264

265 Additionally, the GISS ModelE2.1 was compared to four ATom campaigns (Thompson et al., 2022) of acetone field measurements
266 in the atmosphere (Apel et al., 2021). For this comparison, we averaged the flight data to the model grid, and then compared the
267 resulting mean against the monthly mean fields of the model output. Contrary to other chemical species measured during ATom
268 that vary significantly in space and time, acetone has a rather long lifetime, and the data are collected for the most part very far
269 from its sources. Combining that with the fact that prescribed emissions in the model vary by month, not by day or even hour in
270 GISS ModelE2.1, makes such a comparison appropriate. Meteorology though can affect long-range transport significantly, so for
271 that reason we performed a nudged simulation (called Nudged_ATOM) towards the MERRA-2 reanalysis (Gelaro et al., 2017), to
272 capture such an effect more accurately. We also used emissions and greenhouse gas concentrations from the years of the ATom
273 campaigns and varying with year, rather than the climatological means used in the Baseline simulation. Both the Nudged_ATOM
274 and Baseline simulations are plotted in the ATom comparisons presented here (Figure 10). Although there are some differences at
275 times, for example in the tropical Atlantic Ocean, for the most part the two simulations are indistinguishable, indicating that our
276 conclusions comparing climatological simulations to ATom should be robust. (Figure 10, Figures S4-S6). The GISS ModelE2.1
277 was found to match measurements particularly well in the winter and fall seasons (ATom-2 and ATom-3, respectively). The model
278 underestimated measurements in the mid-northern latitudes in the spring and summer seasons (ATom-4 and ATom-1,
279 respectively), indicating that perhaps the model is not capturing a spring/summer source of acetone in the North. Generally,
280 however, the model matches remote atmosphere measurements remarkably well (Figure 10, Figures S4-S6).

281 3.4 Seasonality of acetone

282 Most European sites presented in Figure 3 have monthly-resolved measurements that can be used to analyze the seasonal behavior
283 of acetone in the model (Figure 11, Figure S7) (Solberg et al., 1996). These sites differ with respect to their geographic locations
284 and their proximity to anthropogenic sources. Zeppelin, Birkenes, Rucava, and Mace Head are all coastal sites, while Waldhof,
285 Kosetice, Donon, Ispra, and Montelibretti are inland sites. Regarding anthropogenic sources, Zeppelin is the most remote location
286 and Birkenes and Rucava each have small sources. Mace Head is a site affected by the marine boundary layer, and Waldhof,
287 Kosetice and Donon are sites with small local anthropogenic sources that are generally located in higher emission regions.
288 Montelibretti and particularly Ispra are subject to the highest anthropogenic sources. The measurements taken at Ispra show an
289 opposite seasonality than what is expected, and previous studies have considered this anomalous (Jacob et al., 2002).

290

291 The GISS ModelE2.1 matches the seasonality of the measurements well, especially in Zeppelin, Mace Head, Waldhof, Kosetice,
292 and Donon. The root mean squared error (RMSE) between the Baseline model and measurements at these five sites are 0.1969,
293 0.0914, 0.3907, 0.3430 and 0.3160, respectively. The model overestimates the measurements in Birkenes and Rucava (RMSE \cong
294 0.87 for both), even though these two sites have low anthropogenic sources. This overestimation has been attributed to the



295 vegetation source, which has a distinct seasonality and is much stronger than any other source there. Interestingly, in Montelibretti,
296 the model's overestimation of vegetation, yet underestimation of local emissions, results in a decent estimation of the sources there
297 (RMSE = 0.5454) (Figure 11).

298

299 As mentioned previously, an analysis of the distribution of the regional sources and sinks at the nine European sites shows that,
300 except for Zeppelin and Mace Head, all studied European sites have vegetation as the dominant source that strongly contributes to
301 the simulated seasonality of concentrations (Figure 12). Vegetation sources peak in the summer months and are lower in the winter.
302 Deposition is a major sink of acetone that is comparable in magnitude with the vegetation source. Ocean uptake of acetone follows
303 a weak seasonal cycle, being stronger in the summer months. The other fluxes (anthropogenic emissions, biomass burning and
304 ocean production) do not exhibit much seasonality at these locations (Figure 12).

305

306 We also compared the GISS ModelE2.1's surface acetone at observation sites with less temporal coverage (Figure 13) (de Gouw
307 et al., 2004; Dolgorouky et al., 2012; Galbally et al., 2007; Guérette et al., 2019; Hu et al., 2013; Huang et al., 2020; Langford et
308 al., 2010; Legrand et al., 2012; Li et al., 2019; Read et al., 2012; Schade & Goldstein, 2006). In general, the GISS ModelE2.1
309 matches the field measurements well. This is especially true for the non-summer seasons in Rosemount and Berkeley, and the
310 summer peaks in Utrecht and Mainz. The model seems to be overestimating acetone around Australia, as shown by comparisons
311 with Cape Grim and Wollongong, while underestimating emissions in large cities like Shenzhen, Beijing, London, and Paris.

312 **3.5 Sensitivity studies**

313 The sensitivity simulations presented here have been described in section 2.5 and in Table 1. We grouped them in two categories:
314 those directly related with chemical sources and sinks, and those related with terrestrial and oceanic acetone fluxes. Overall, the
315 sensitivity studies that presented large changes to total atmospheric burden included Chem_Terp0, Chem_Par0.5, Chem_Par2.0,
316 Veg_0.7, Ocn_2.0, and Dep_f00 (all but Chem_ClO and BB_2.0) (Figures S8-S13).

317 **3.5.1 Chemistry**

318 Chemistry sensitivity tests that modified the sources of acetone were analyzed with respect to the budget and global distribution
319 of acetone. In the Chem_ClO simulation, where no acetone oxidation by the chlorine radical occurs, the overall global acetone
320 budget does not change. However, in some places like Rucava, Ispra, Montelibretti, and Shenzhen, the shape of the acetone
321 concentration profile over the year changes slightly (Figure 14, Figure S14). The Chem_Terp0 simulation that removes the
322 production of acetone from terpenes decreases the summer peak of acetone by as much as 35.5% in Birkenes, 25.5% in Mainz,
323 and 25.3% in Berkeley (Figure 14, Figure S14). Other sites like Montelibretti, Ispra and Paris have their summer peak decreased
324 by 22.6%, 22.2%, and 19.0%, respectively (Figure 14, Figure S14). Coastal and remote areas like Zeppelin, Mace Head and
325 Dumont d'Urville are not impacted by the removal of terpenes (Figure 14, Figure S14). There seems to be some nonlinearities
326 with the relationship between acetone abundance and its yield from paraffin, as the results from the Chem_Par2.0 and Chem_Par0.5
327 simulation reveal that doubling the yield has a stronger impact than halving it. For instance, in Montelibretti, doubling the yield
328 from paraffin increases the summer peak by 35.7%, while halving the yield decreases the summer peak by only 8.3% (Figure 14,
329 Figure S14). A similar relationship is observed at other sites: Ispra (19.1% increase with double paraffin, 2.5% decrease with half
330 paraffin) and Berkeley (12.7% increase with double paraffin, 2.5% decrease with half paraffin) (Figure 14, Figure S14). Overall,
331 we explored chemistry sensitivities that would tend to push acetone in both directions. The Baseline simulation falls between our
332 tests, which we have identified as important uncertainties.



333

334 The spatial distribution differences between the chemistry sensitivity studies and the Baseline simulation show some interesting
335 patterns (Figure 15). Removing the production of acetone from terpenes oxidation decreased acetone over the continents, and
336 especially over tropical and boreal forests which are where terpenes are emitted. This change induced a feedback where acetone
337 concentration increased slightly over the oceans (Figure 15, top left). Halving production of acetone from paraffin oxidation only
338 decreased acetone concentrations over the continents (Figure 15, top right), while doubling it increased acetone concentrations
339 over the continents but reduced it marginally downwind (Figure 15, bottom). Feedback resulting from this change was that acetone
340 destruction increased over the tropics.

341 **3.5.2 Terrestrial and oceanic fluxes**

342 Terrestrial and oceanic fluxes sensitivities were analyzed at the same sites. The vegetation flux sensitivity, Veg_0.7, reduced
343 acetone production from MEGAN by 30%. This change decreased the summer peak of acetone down at nearly every location
344 studied, but most notably by 32.6% in Birkenes, 22.9% in Rucava, and 22.2% in Rosemount (Figure 16, Figure S15).

345

346 In the oceanic flux sensitivity simulation, Ocn_2.0, the concentration of acetone in the water was doubled from 15 nM to 30 nM.
347 The results of this simulation varied with geographic location. For instance, in Birkenes, doubling ocean concentration reduced
348 overall acetone by 13.9%, while in Montelibretti, it was increased by 16.1% (Figure 16). Even though Birkenes is more of a
349 coastal city than Montelibretti, this result may simply be a temperature effect; Birkenes is at 58°N, while Montelibretti is at
350 42°N, and a warmer ocean may produce more acetone. Overall, in most places, the doubling ocean acetone concentration did not
351 change much atmospheric acetone throughout the year.

352

353 Another broader finding from the ocean sensitivity study is that doubling the ocean acetone concentration impacted oceanic
354 emissions of acetone more than the oceanic uptake of acetone. Specifically, in this sensitivity study the emissions doubled, while
355 the uptake only increased by 40%. This difference may be attributed to the fact that a higher ocean concentration will generally
356 cause less resistance in the emission direction, but more resistance in the uptake direction. The differences in oceanic acetone
357 emissions and uptakes in this sensitivity study also resulted in increased chemical destruction, and an overall higher burden of
358 acetone in the atmosphere (Figure S12).

359

360 In the dry deposition sensitivity simulation, the reactivity factor, f_0 , was reduced from 0.1 to 0. As a result, the amount of acetone
361 removed by deposition decreased, and the atmospheric acetone concentration increased. The strongest increases were found to be
362 in Ispra (38.4% increase), Kosetice (37.9% increase), Paris (37.9% increase), Beijing (37.3% increase), Donon (36.6% increase),
363 Mainz (33.4% increase), Montelibretti (30.5% increase), Rosemount (28.9% increase), Berkeley (28.7% increase), and Waldhof
364 (28.7% increase) (Figure 16, Figure S14). The final terrestrial fluxes sensitivity study, BB_2.0, doubled biomass burning emissions.
365 This sensitivity did not significantly change acetone mixing ratios in any of the locations studied, except an increased summer
366 spike (12.7% increase) in Birkenes (Figure 16). Most of the locations studied were far from biomass burning sites to begin with,
367 however, so an analysis of this sensitivity study over biomass burning hotspots is needed.

368

369 The acetone concentration anomalies around the world between the terrestrial and oceanic fluxes sensitivity studies and the
370 Baseline simulation are presented in Figure 17. Decreasing acetone production from MEGAN vegetation by 30% resulted in a
371 decrease of acetone mixing ratios over the tropical and boreal forests, where this source is most prominent (Figure 17, top left).



372 Doubling ocean acetone concentrations increased production of acetone from the oceans globally. This increase was stronger in
373 the tropics, due to the higher sea surface temperatures (Figure 17, top right). Reducing the reactivity factor for dry deposition
374 decreased the amount of acetone removed by deposition over the continents (Figure 17, bottom left), in particular where acetone
375 concentration is elevated (Figure 3). Finally, doubling biomass burning emissions did not change acetone mixing ratios much,
376 other than over biomass burning hotspots like central South America, central Africa, Southeast Asia, and Siberia (Figure 17, bottom
377 right).

378 3.5.3 ATom comparisons

379 The ATom comparisons were replicated with the sensitivity simulations (Figure 18, Figures S16-S18). Doubling the paraffin yield
380 and doubling the ocean acetone concentration seemed to have the most noticeable impacts on the vertical profiles. As seen in the
381 summer season (ATom-1), doubling the paraffin yield more closely matches the measurements in the Northern hemisphere remote
382 atmosphere (Figure 18). In the fall season (ATom-3), however, doubling the paraffin yield tends to overshoot most of the
383 measurements (Figure S17). These results reveal that the model may be missing a paraffin source that is active during the summer
384 season, and a paraffin sink that is active in the fall season. Additionally, the ocean sensitivity tends to shift the vertical profile right
385 (overshooting measurements) in nearly all locations of the winter season (ATom-2), and in the Southern hemisphere of the other
386 seasons. While the ocean flux may be small, these ATom comparisons reveal that they especially matter in the southern latitudes.
387 These are the same latitudes where the ocean appears to be in equilibrium (neither a strong source nor sink) (Figure 7).

388 4 Conclusion

389 The development of acetone's representation in the NASA GISS ModelE2.1 from its previous simplistic parameterization of
390 instantaneous isoprene to a full tracer experiencing transport, chemistry, emissions, and deposition of its own, marks a significant
391 improvement to the model's chemical scheme. Calculations of the 3-dimensional distribution of acetone as a function of time, as
392 well as evaluations of its atmospheric burden and source/sink fluxes demonstrate the complexity of acetone's spatiotemporal
393 distribution in the atmosphere. An extensive analysis was conducted to assess the simulated global acetone budget in the context
394 of past modeling studies. Further comparisons were made against field measurements on a variety of spatial and temporal scales,
395 which indicated that the model agrees well with surface field measurements and vertical profiles in the remote atmosphere. The
396 chemical formation of acetone from precursor compounds such as paraffin was found to be an uncertain yet impactful factor.
397 Vegetation fluxes as calculated by MEGAN were identified as the dominant acetone source which dictates its seasonality.
398 Additionally, the acetone concentration in seawater was found to affect oceanic sources more than oceanic sinks.

399

400 The work presented here demonstrates the usefulness of the approach to evaluate a chemical species in the model, and can be used
401 for similar evaluations of other important gaseous and aerosol species. Any feedback between acetone and the rest of the chemistry,
402 and particularly ozone, have not been assessed here, and should be the goal of a future study. Additionally, the current ocean-
403 acetone interaction uses a constant concentration of acetone in the ocean. It will be helpful to test a more realistic, non-uniform
404 ocean acetone concentration, when this becomes available. Finally, other atmospheric conditions such as surface wind speed may
405 be considered further when modifying the ocean scheme.



406 **Code Availability**

407 The GISS ModelE code is publicly available at <https://simplex.giss.nasa.gov/snapshots/>. The most recent public version is E.2.1.2;
408 the version of the code used here is already committed in the non-public-facing repository and will be released in the future
409 following the regular release cycle of ModelE, under version E3.1. The code used for the simulations described here, including the
410 configuration scripts (“rundecks”) used to perform the simulations, are available together with the model output and scripts used
411 to generate plots, here: <https://doi.org/10.5281/zenodo.7954593>.

412 **Data Availability**

413 We have made available the simulated three-dimensional distributions of acetone from each simulation described in the paper
414 (Baseline, sensitivity simulations in Table 1, and Nudged_ATOM). These are found in zip files, grouped by simulation, together
415 with the model code and scripts used to generate plots, here: <https://doi.org/10.5281/zenodo.7954593>. Each zip file contains a
416 series of netCDF format files with filenames {month}_5yrAvg_Acetone_{simulation}.nc, where each file is a climatological
417 average over 5 years of repeated forcing conditions.

418

419 The exception is the transient-forcing simulation "Nudged_ATOM", which contains single-month averages of acetone from JUL
420 2016 through MAY 2018, to cover the ATom observational period. The file names for that simulation are of the form:
421 {month}_{year}_Acetone_Nudged_ATOM.nc. Acetone is in ppbv units and given on the model's native grid and vertical levels.
422 These are hybrid sigma levels, but nominal pressure middles and edges are given in the plm and ple variables, respectively, and
423 the grid box surface areas are also provided.

424 **Author Contribution**

425 KT conceived the study and guided the model development which was done by GF. All simulations presented here were performed
426 by GF. DS advised during the whole development process. AR did the literature search and all comparisons against other modeling
427 studies. With the exception of the ATom analysis and plots which were done by KT, and comparisons against field measurements
428 and the rest of the plots were done by AR. AR drafted the first version of the manuscript, and all authors contributed to it. GF
429 prepared all model outputs for dissemination.

430 **Competing Interests**

431 The authors declare that they have no conflict of interest.

432 **Acknowledgements**

433 Climate modeling at GISS is supported by the NASA Modeling, Analysis and Prediction program. AR acknowledges support from
434 North Carolina Space Grant and the NASA Office of STEM Engagement. Resources supporting this work were provided by the
435 NASA High-End Computing (HEC) Program through the NASA Center for Climate Simulation (NCCS) at Goddard Space Flight
436 Center.



437 **References**

- 438 Apel, E. C., Asher, E. C., Hills, A. J., and Hornbrook, R. S.: ATom: Volatile Organic Compounds (VOCs) from the TOGA
439 instrument, Version 2, ORNL DAAC, <https://doi.org/10.3334/ORNLDAAC/1936>, 2021.
- 440 Arnold, S. R., Chipperfield, M. P., and Blitz, M. A.: A three-dimensional model study of the effect of new temperature-dependent
441 quantum yields for acetone photolysis, *J. Geophys. Res. Atmospheres*, 110, <https://doi.org/10.1029/2005JD005998>, 2005.
- 442 Beale, R., Dixon, J. L., Arnold, S. R., Liss, P. S., and Nightingale, P. D.: Methanol, acetaldehyde, and acetone in the surface waters
443 of the Atlantic Ocean, *J. Geophys. Res. Oceans*, 118, 5412–5425, <https://doi.org/10.1002/jgrc.20322>, 2013.
- 444 Benkelberg, H.-J., Hamm, S., and Warneke, P.: Henry's law coefficients for aqueous solutions of acetone, acetaldehyde and
445 acetonitrile, and equilibrium constants for the addition compounds of acetone and acetaldehyde with bisulfite, *J. Atmospheric
446 Chem.*, 20, 17–34, <https://doi.org/10.1007/BF01099916>, 1995.
- 447 Brewer, J. F., Bishop, M., Kelp, M., Keller, C. A., Ravishankara, A. R., and Fischer, E. V.: A sensitivity analysis of key natural
448 factors in the modeled global acetone budget, *J. Geophys. Res. Atmospheres*, 122, 2043–2058,
449 <https://doi.org/10.1002/2016JD025935>, 2017.
- 450 Chin, M., Jacob, D. J., Gardner, G. M., Foreman-Fowler, M. S., Spiro, P. A., and Savoie, D. L.: A global three-dimensional model
451 of tropospheric sulfate, *J. Geophys. Res. Atmospheres*, 101, 18667–18690, <https://doi.org/10.1029/96JD01221>, 1996.
- 452 Dolgorouky, C., Gros, V., Sarda-Esteve, R., Sinha, V., Williams, J., Marchand, N., Sauvage, S., Poulain, L., Sciare, J., and
453 Bonsang, B.: Total OH reactivity measurements in Paris during the 2010 MEGAPOLI winter campaign, *Atmospheric Chem. Phys.*,
454 12, 9593–9612, <https://doi.org/10.5194/acp-12-9593-2012>, 2012.
- 455 Dufour, G., Szopa, S., Harrison, J. J., Boone, C. D., and Bernath, P. F.: Seasonal variations of acetone in the upper troposphere–
456 lower stratosphere of the northern midlatitudes as observed by ACE-FTS, *J. Mol. Spectrosc.*, 323, 67–77,
457 <https://doi.org/10.1016/j.jms.2016.02.006>, 2016.
- 458 Elias, T., Szopa, S., Zahn, A., Schuck, T., Brenninkmeijer, C., Sprung, D., and Slemr, F.: Acetone variability in the upper
459 troposphere: analysis of CARIBIC observations and LMDz-INCA chemistry-climate model simulations, *Atmospheric Chem.
460 Phys.*, 11, 8053–8074, <https://doi.org/10.5194/acp-11-8053-2011>, 2011.
- 461 Fischbeck, G., Bönisch, H., Neumaier, M., Brenninkmeijer, C. A. M., Orphal, J., Brito, J., Becker, J., Sprung, D., van Velthoven,
462 P. F. J., and Zahn, A.: Acetone–CO enhancement ratios in the upper troposphere based on 7 years of CARIBIC data: new insights
463 and estimates of regional acetone fluxes, *Atmospheric Chem. Phys.*, 17, 1985–2008, <https://doi.org/10.5194/acp-17-1985-2017>,
464 2017.
- 465 Fischer, E. V., Jacob, D. J., Millet, D. B., Yantosca, R. M., and Mao, J.: The role of the ocean in the global atmospheric budget of
466 acetone, *Geophys. Res. Lett.*, 39, <https://doi.org/10.1029/2011GL050086>, 2012.
- 467 Folberth, G. A., Hauglustaine, D. A., Lathière, J., and Brocheton, F.: Interactive chemistry in the Laboratoire de Météorologie
468 Dynamique general circulation model: model description and impact analysis of biogenic hydrocarbons on tropospheric chemistry,
469 *Atmospheric Chem. Phys.*, 6, 2273–2319, <https://doi.org/10.5194/acp-6-2273-2006>, 2006.
- 470 Galbally, I., Lawson, S. J., Bentley, S., Gillett, R., Meyer, M., and Goldstein, A.: Volatile organic compounds in marine air at Cape
471 Grim, Australia, *Environ. Chem. - Env. CHEM*, 4, <https://doi.org/10.1071/EN07024>, 2007.
- 472 Gelaro, R., McCarty, W., Suárez, M. J., Todling, R., Molod, A., Takacs, L., Randles, C. A., Darmenov, A., Bosilovich, M. G.,
473 Reichle, R., Wargan, K., Coy, L., Cullather, R., Draper, C., Akella, S., Buchard, V., Conaty, A., Silva, A. M. da, Gu, W., Kim, G.-
474 K., Koster, R., Lucchesi, R., Merkova, D., Nielsen, J. E., Partyka, G., Pawson, S., Putman, W., Rienecker, M., Schubert, S. D.,
475 Sienkiewicz, M., and Zhao, B.: The Modern-Era Retrospective Analysis for Research and Applications, Version 2 (MERRA-2),
476 *J. Clim.*, 30, 5419–5454, <https://doi.org/10.1175/JCLI-D-16-0758.1>, 2017.
- 477 de Gouw, J., Warneke, C., Holzinger, R., Klüpfel, T., and Williams, J.: Inter-comparison between airborne measurements of
478 methanol, acetonitrile and acetone using two differently configured PTR-MS instruments, *Int. J. Mass Spectrom.*, 239, 129–137,
479 <https://doi.org/10.1016/j.ijms.2004.07.025>, 2004.



- 480 Guenther, A. B., Jiang, X., Heald, C. L., Sakulyanontvittaya, T., Duhl, T., Emmons, L. K., and Wang, X.: The Model of Emissions
481 of Gases and Aerosols from Nature version 2.1 (MEGAN2.1): an extended and updated framework for modeling biogenic
482 emissions, *Geosci. Model Dev.*, 5, 1471–1492, <https://doi.org/10.5194/gmd-5-1471-2012>, 2012.
- 483 Guérette, É.-A., Paton-Walsh, C., Galbally, I., Molloy, S., Lawson, S., Kubistin, D., Buchholz, R., Griffith, D. W. T., Langenfelds,
484 R. L., Krummel, P. B., Loh, Z., Chambers, S., Griffiths, A., Keywood, M., Selleck, P., Dominick, D., Humphries, R., and Wilson,
485 S. R.: Composition of Clean Marine Air and Biogenic Influences on VOCs during the MUMBA Campaign, *Atmosphere*, 10, 383,
486 <https://doi.org/10.3390/atmos10070383>, 2019.
- 487 Hu, L., Millet, D. B., Kim, S. Y., Wells, K. C., Griffis, T. J., Fischer, E. V., Helmig, D., Hueber, J., and Curtis, A. J.: North
488 American acetone sources determined from tall tower measurements and inverse modeling, *Atmospheric Chem. Phys.*, 13, 3379–
489 3392, <https://doi.org/10.5194/acp-13-3379-2013>, 2013.
- 490 Huang, X.-F., Zhang, B., Xia, S.-Y., Han, Y., Wang, C., Yu, G.-H., and Feng, N.: Sources of oxygenated volatile organic
491 compounds (OVOCs) in urban atmospheres in North and South China, *Environ. Pollut.*, 261, 114152,
492 <https://doi.org/10.1016/j.envpol.2020.114152>, 2020.
- 493 Jacob, D. J., Field, B. D., Jin, E. M., Bey, I., Li, Q., Logan, J. A., Yantosca, R. M., and Singh, H. B.: Atmospheric budget of
494 acetone, *J. Geophys. Res. Atmospheres*, 107, ACH 5-1-ACH 5-17, <https://doi.org/10.1029/2001JD000694>, 2002.
- 495 Johnson, M. T.: A numerical scheme to calculate temperature and salinity dependent air-water transfer velocities for any gas,
496 *Ocean Sci.*, 6, 913–932, <https://doi.org/10.5194/os-6-913-2010>, 2010.
- 497 Kelley, M., Schmidt, G. A., Nazarenko, L. S., Bauer, S. E., Ruedy, R., Russell, G. L., Ackerman, A. S., Aleinov, I., Bauer, M.,
498 Bleck, R., Canuto, V., Cesana, G., Cheng, Y., Clune, T. L., Cook, B. I., Cruz, C. A., Genio, A. D. D., Elsaesser, G. S., Falu vegi,
499 G., Kiang, N. Y., Kim, D., Lacis, A. A., Leboissetier, A., LeGrande, A. N., Lo, K. K., Marshall, J., Matthews, E. E., McDermid,
500 S., Mezuman, K., Miller, R. L., Murray, L. T., Oinas, V., Orbe, C., García-Pando, C. P., Perlwitz, J. P., Puma, M. J., Rind, D.,
501 Romanou, A., Shindell, D. T., Sun, S., Tausnev, N., Tsigaridis, K., Tselioudis, G., Weng, E., Wu, J., and Yao, M.-S.: GISS-E2.1:
502 Configurations and Climatology, *J. Adv. Model. Earth Syst.*, 12, e2019MS002025, <https://doi.org/10.1029/2019MS002025>, 2020.
- 503 Khan, M. A. H., Cooke, M. C., Utembe, S. R., Archibald, A. T., Maxwell, P., Morris, W. C., Xiao, P., Derwent, R. G., Jenkin, M.
504 E., Percival, C. J., Walsh, R. C., Young, T. D. S., Simmonds, P. G., Nickless, G., O'Doherty, S., and Shallcross, D. E.: A study of
505 global atmospheric budget and distribution of acetone using global atmospheric model STOCHEM-CRI, *Atmos. Environ.*, 112,
506 269–277, <https://doi.org/10.1016/j.atmosenv.2015.04.056>, 2015.
- 507 Langford, B., Nemitz, E., House, E., Phillips, G. J., Famulari, D., Davison, B., Hopkins, J. R., Lewis, A. C., and Hewitt, C. N.:
508 Fluxes and concentrations of volatile organic compounds above central London, UK, *Atmospheric Chem. Phys.*, 10, 627–645,
509 <https://doi.org/10.5194/acp-10-627-2010>, 2010.
- 510 Legrand, M., Gros, V., Preunkert, S., Sarda-Estève, R., Thierry, A.-M., Pépy, G., and Jourdain, B.: A reassessment of the budget
511 of formic and acetic acids in the boundary layer at Dumont d'Urville (coastal Antarctica): The role of penguin emissions on the
512 budget of several oxygenated volatile organic compounds, *J. Geophys. Res. Atmospheres*, 117,
513 <https://doi.org/10.1029/2011JD017102>, 2012.
- 514 Lewis, A. C., Hopkins, J. R., Carpenter, L. J., Stanton, J., Read, K. A., and Pilling, M. J.: Sources and sinks of acetone, methanol,
515 and acetaldehyde in North Atlantic marine air, *Atmospheric Chem. Phys.*, 5, 1963–1974, <https://doi.org/10.5194/acp-5-1963-2005>,
516 2005.
- 517 Li, K., Li, J., Tong, S., Wang, W., Huang, R.-J., and Ge, M.: Characteristics of wintertime VOCs in suburban and urban Beijing:
518 concentrations, emission ratios, and festival effects, *Atmospheric Chem. Phys.*, 19, 8021–8036, <https://doi.org/10.5194/acp-19-8021-2019>, 2019.
- 520 Liss, P. S.: Processes of gas exchange across an air-water interface, *Deep Sea Res. A*, 20, 221–238, [https://doi.org/10.1016/0011-7471\(73\)90013-2](https://doi.org/10.1016/0011-7471(73)90013-2), 1973.
- 522 Marandino, C. A., Bruyn, W. J. D., Miller, S. D., Prather, M. J., and Saltzman, E. S.: Oceanic uptake and the global atmospheric
523 acetone budget, *Geophys. Res. Lett.*, 32, <https://doi.org/10.1029/2005GL023285>, 2005.
- 524 Read, K. A., Carpenter, L. J., Arnold, S. R., Beale, R., Nightingale, P. D., Hopkins, J. R., Lewis, A. C., Lee, J. D., Mendes, L., and
525 Pickering, S. J.: Multiannual Observations of Acetone, Methanol, and Acetaldehyde in Remote Tropical Atlantic Air: Implications



- 526 for Atmospheric OVOC Budgets and Oxidative Capacity, *Environ. Sci. Technol.*, 46, 11028–11039,
527 <https://doi.org/10.1021/es302082p>, 2012.
- 528 Sander, R.: Compilation of Henry's Law Constants for Inorganic and Organic Species of Potential Importance in Environmental
529 Chemistry, n.d.
- 530 Sander, S. P., Friedl, R. R., Barker, J. R., Abbatt, J. P. D., and Burkholder, J. B.: Chemical Kinetics and Photochemical Data for
531 Use in Atmospheric Studies Evaluation Number 17, n.d.
- 532 Schade, G. W. and Goldstein, A. H.: Seasonal measurements of acetone and methanol: Abundances and implications for
533 atmospheric budgets, *Glob. Biogeochem. Cycles*, 20, <https://doi.org/10.1029/2005GB002566>, 2006.
- 534 Shindell, D. T., Grenfell, J. L., Rind, D., Grewe, V., and Price, C.: Chemistry-climate interactions in the Goddard Institute for
535 Space Studies general circulation model: 1. Tropospheric chemistry model description and evaluation, *J. Geophys. Res.*
536 *Atmospheres*, 106, 8047–8075, <https://doi.org/10.1029/2000JD900704>, 2001.
- 537 Shindell, D. T., Faluvegi, G., and Bell, N.: Preindustrial-to-present-day radiative forcing by tropospheric ozone from improved
538 simulations with the GISS chemistry-climate GCM, *Atmospheric Chem. Phys.*, 3, 1675–1702, [https://doi.org/10.5194/acp-3-1675-](https://doi.org/10.5194/acp-3-1675-2003)
539 2003, 2003.
- 540 Singh, H., Chen, Y., Tabazadeh, A., Fukui, Y., Bey, I., Yantosca, R., Jacob, D., Arnold, F., Wohlfrom, K., Atlas, E., Flocke, F.,
541 Blake, D., Blake, N., Heikes, B., Snow, J., Talbot, R., Gregory, G., Sachse, G., Vay, S., and Kondo, Y.: Distribution and fate of
542 selected oxygenated organic species in the troposphere and lower stratosphere over the Atlantic, *J. Geophys. Res. Atmospheres*,
543 105, 3795–3805, <https://doi.org/10.1029/1999JD900779>, 2000.
- 544 Singh, H. B., O'Hara, D., Herlth, D., Sachse, W., Blake, D. R., Bradshaw, J. D., Kanakidou, M., and Crutzen, P. J.: Acetone in the
545 atmosphere: Distribution, sources, and sinks, *J. Geophys. Res. Atmospheres*, 99, 1805–1819, <https://doi.org/10.1029/93JD00764>,
546 1994.
- 547 Singh, H. B., Tabazadeh, A., Evans, M. J., Field, B. D., Jacob, D. J., Sachse, G., Crawford, J. H., Shetter, R., and Brune, W. H.:
548 Oxygenated volatile organic chemicals in the oceans: Inferences and implications based on atmospheric observations and air-sea
549 exchange models, *Geophys. Res. Lett.*, 30, <https://doi.org/10.1029/2003GL017933>, 2003.
- 550 Singh, H. B., Salas, L. J., Chatfield, R. B., Czech, E., Fried, A., Walega, J., Evans, M. J., Field, B. D., Jacob, D. J., Blake, D.,
551 Heikes, B., Talbot, R., Sachse, G., Crawford, J. H., Avery, M. A., Sandholm, S., and Fuelberg, H.: Analysis of the atmospheric
552 distribution, sources, and sinks of oxygenated volatile organic chemicals based on measurements over the Pacific during TRACE-
553 P, *J. Geophys. Res. Atmospheres*, 109, <https://doi.org/10.1029/2003JD003883>, 2004.
- 554 Solberg, S., Dye, C., Schmidbauer, N., Herzog, A., and Gehrig, R.: Carbonyls and nonmethane hydrocarbons at rural European
555 sites from the mediterranean to the arctic, *J. Atmospheric Chem.*, 25, 33–66, <https://doi.org/10.1007/BF00053285>, 1996.
- 556 Thompson, C. R., Wofsy, S. C., Prather, M. J., Newman, P. A., Hanisco, T. F., Ryerson, T. B., Fahey, D. W., Apel, E. C., Brock,
557 C. A., Brune, W. H., Froyd, K., Katich, J. M., Nicely, J. M., Peischl, J., Ray, E., Veres, P. R., Wang, S., Allen, H. M., Asher, E.,
558 Bian, H., Blake, D., Bourgeois, I., Budney, J., Bui, T. P., Butler, A., Campuzano-Jost, P., Chang, C., Chin, M., Commane, R.,
559 Correa, G., Crounse, J. D., Daube, B., Dibb, J. E., DiGangi, J. P., Diskin, G. S., Dollner, M., Elkins, J. W., Fiore, A. M., Flynn, C.
560 M., Guo, H., Hall, S. R., Hannun, R. A., Hills, A., Hints, E. J., Hodzic, A., Hornbrook, R. S., Huey, L. G., Jimenez, J. L., Keeling,
561 R. F., Kim, M. J., Kupc, A., Lacey, F., Lait, L. R., Lamarque, J.-F., Liu, J., McKain, K., Meinardi, S., Miller, D. O., Montzka, S.
562 A., Moore, F. L., Morgan, E. J., Murphy, D. M., Murray, L. T., Nault, B. A., Neuman, J. A., Nguyen, L., Gonzalez, Y., Rollins,
563 A., Rosenlof, K., Sargent, M., Schill, G., Schwarz, J. P., Clair, J. M. S., Steenrod, S. D., Stephens, B. B., Strahan, S. E., Strode, S.
564 A., Sweeney, C., Thames, A. B., Ullmann, K., Wagner, N., Weber, R., Weinzierl, B., Wennberg, P. O., Williamson, C. J., Wolfe,
565 G. M., and Zeng, L.: The NASA Atmospheric Tomography (ATom) Mission: Imaging the Chemistry of the Global Atmosphere,
566 *Bull. Am. Meteorol. Soc.*, 103, E761–E790, <https://doi.org/10.1175/BAMS-D-20-0315.1>, 2022.
- 567 Tsigaridis, K. and Kanakidou, M.: Global modelling of secondary organic aerosol in the troposphere: a sensitivity analysis, *Atmos*
568 *Chem Phys*, 2003.
- 569 Wang, S., Apel, E. C., Schwantes, R. H., Bates, K. H., Jacob, D. J., Fischer, E. V., Hornbrook, R. S., Hills, A. J., Emmons, L. K.,
570 Pan, L. L., Honomichl, S., Tilmes, S., Lamarque, J.-F., Yang, M., Marandino, C. A., Saltzman, E. S., Bruyn, W. de, Kameyama,
571 S., Tanimoto, H., Omori, Y., Hall, S. R., Ullmann, K., Ryerson, T. B., Thompson, C. R., Peischl, J., Daube, B. C., Commane, R.,
572 McKain, K., Sweeney, C., Thames, A. B., Miller, D. O., Brune, W. H., Diskin, G. S., DiGangi, J. P., and Wofsy, S. C.: Global



573 Atmospheric Budget of Acetone: Air-Sea Exchange and the Contribution to Hydroxyl Radicals, *J. Geophys. Res. Atmospheres*,
 574 125, e2020JD032553, <https://doi.org/10.1029/2020JD032553>, 2020.

575 Warneke, C. and de Gouw, J. A.: Organic trace gas composition of the marine boundary layer over the northwest Indian Ocean in
 576 April 2000, *Atmos. Environ.*, 35, 5923–5933, [https://doi.org/10.1016/S1352-2310\(01\)00384-3](https://doi.org/10.1016/S1352-2310(01)00384-3), 2001.

577 Weimer, M., Schröter, J., Eckstein, J., Deetz, K., Neumaier, M., Fischbeck, G., Hu, L., Millet, D. B., Rieger, D., Vogel, H., Vogel,
 578 B., Reddmann, T., Kirner, O., Ruhnke, R., and Braesicke, P.: An emission module for ICON-ART 2.0: implementation and
 579 simulations of acetone, *Geosci. Model Dev.*, 10, 2471–2494, <https://doi.org/10.5194/gmd-10-2471-2017>, 2017.

580 Wesely, M. L. and Hicks, B. B.: Some Factors that Affect the Deposition Rates of Sulfur Dioxide and Similar Gases on Vegetation,
 581 *J. Air Pollut. Control Assoc.*, 27, 1110–1116, <https://doi.org/10.1080/00022470.1977.10470534>, 1977.

582 Yoshino, A., Nakashima, Y., Miyazaki, K., Kato, S., Suthawaree, J., Shimo, N., Matsunaga, S., Chatani, S., Apel, E., Greenberg,
 583 J., Guenther, A., Ueno, H., Sasaki, H., Hoshi, J., Yokota, H., Ishii, K., and Kajii, Y.: Air quality diagnosis from comprehensive
 584 observations of total OH reactivity and reactive trace species in urban central Tokyo, *Atmos. Environ.*, 49, 51–59,
 585 <https://doi.org/10.1016/j.atmosenv.2011.12.029>, 2012.

586 Yuan, B., Hu, W. W., Shao, M., Wang, M., Chen, W. T., Lu, S. H., Zeng, L. M., and Hu, M.: VOC emissions, evolutions and
 587 contributions to SOA formation at a receptor site in eastern China, *Atmospheric Chem. Phys.*, 13, 8815–8832,
 588 <https://doi.org/10.5194/acp-13-8815-2013>, 2013.

589 Zhou, X. and Mopper, K.: Apparent partition coefficients of 15 carbonyl compounds between air and seawater and between air
 590 and freshwater; implications for air-sea exchange, *Environ. Sci. Technol.*, 24, 1864–1869, <https://doi.org/10.1021/es00082a013>,
 591 1990.

592 **Tables and Figures**

593 **Table 1.** Sensitivity studies conducted to observe the leverage a specific parameter afforded the model. Simulation names, as well
 594 as the parameter they target and a description, are included.

GISS ModelE2.1 Sensitivity Simulation	Sensitivity Parameter	Description
Chem_Cl0	Chemistry Source	Acetone + Chlorine reaction rate = 0
Chem_Terp0	Chemistry Source	No reaction for production of acetone from terpenes
Chem_Par0.5	Chemistry Source	Half the yield of acetone from paraffin (17.5%)
Chem_Par2.0	Chemistry Source	Double the yield of acetone from paraffin (70%)
Veg_0.7	Vegetation	0.7 factor of acetone from MEGAN
Ocn_2.0	Ocean	Ocean acetone concentration from 15nM to 30nM
Dep_f0	Dry Deposition	f ₀ changed from 0.1 to 0
BB_2.0	Biomass Burning	Double biomass burning emissions

595
 596 **Table 2.** Global acetone budget table comparing burden, flux and lifetime estimates of acetone from the Baseline model to thirteen
 597 previous studies.

	Wang <i>et al.</i> [2020] ^a	Wang <i>et al.</i> [2020] ^b	Brewer <i>et al.</i> [2017]	Fischer <i>et al.</i> [2012]	Elias <i>et al.</i> [2011]	Jacob <i>et al.</i> [2002]	Other Estimates [2000-2016] ^c



Burden (Tg)	3.5	3.80	5.57	5.60	7.20	3.80	3.50 – 4.20
Global Deposition (Tg yr ⁻¹)	-25.2	-12.4	-12.4	-12.0	-19.0	-9.0	-26.0 – -6.0
Biomass Burning (Tg yr ⁻¹)	4.0	2.40	2.60	2.80	2.40	4.50	3.22 – 9.0
Anthro Emissions (Tg yr ⁻¹)	0.50	3.40	3.60	0.73	1.60	1.10	1.02 – 2.0
Vegetation Emissions (Tg yr ⁻¹)	39.8	32.2	37.1	32.0	76.0	35.0	15 – 56
Net Ocean (Tg yr ⁻¹)	-8.10	1.30	-7.50	-2.0	-8.0	13.0	4.0
Ocean Source (Tg yr ⁻¹)	33.4	45.7	51.8	80.0	20.0	27.0	20.0
Ocean Sink (Tg yr ⁻¹)	-41.5	-44.4	-59.2	-82.0	-28.0	-14.0	-62.0
Net Chemistry (Tg yr ⁻¹)	-11.1	-26.1	-22.5	-21.0	-53.0	-45.0	-33.0 – -5.50
Chem Source (Tg yr ⁻¹)	38.5	26.1	24.1	31.0	27.0	28.0	15.5 – 55.6
Chem Sink (Tg yr ⁻¹)	-49.6	-52.2	-46.6	-52.0	-80.0	-73.0	-61.1 – -33.4
Chemical Lifetime (days) ^c	25.8	26.6	43.6	39.3	32.9	19.0	20.9 – 35.6
Lifetime (days) ^d	11.0	12.7	17.2	14.0	21.0	14.5	12.8 – 35

^a CAM-Chem Model (Wang et al., 2020)

^b GEOS-Chem Model (Wang et al., 2020)

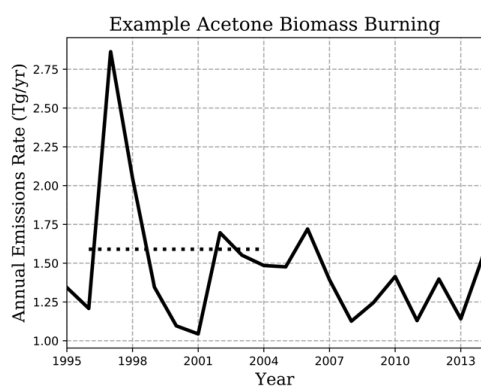
^c Chemical Lifetime = Burden/Chemical Sink

^d Total Atmospheric Lifetime = Burden/Total Sink

^e Singh et al. [2000, 2004], Arnold et al. [2005], Folberth et al. [2006], Marandino et al. [2006], Guenther et al. [2012], Beale et al. [2013], Khan et al. [2015], Dufour et al. [2016].

598

599



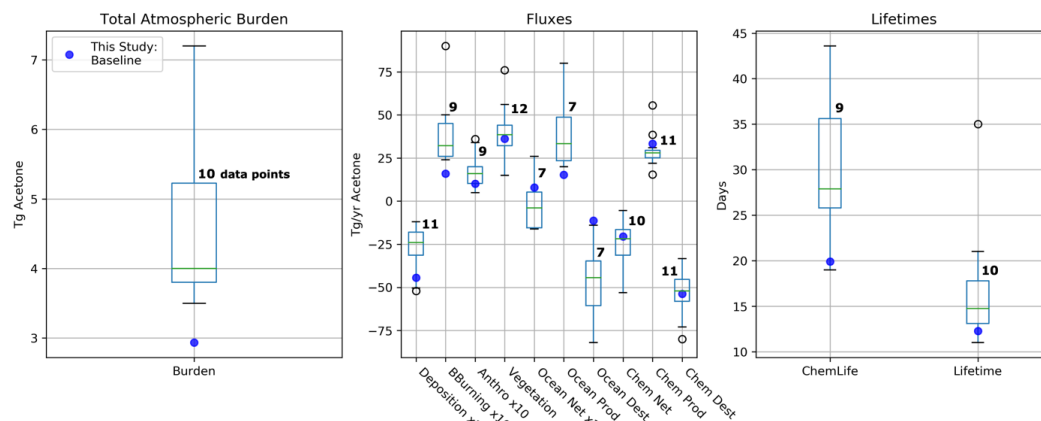
600

601 **Figure 1.** Illustration of interannual variability of NMVOC-C₃H₆ biomass burning emissions of van Marle et al., 2017 (solid line),

602 used as acetone emissions in our simulation. Climatological-emissions simulations use the 1996-2004 mean (dotted line), though

603 emissions vary with month.

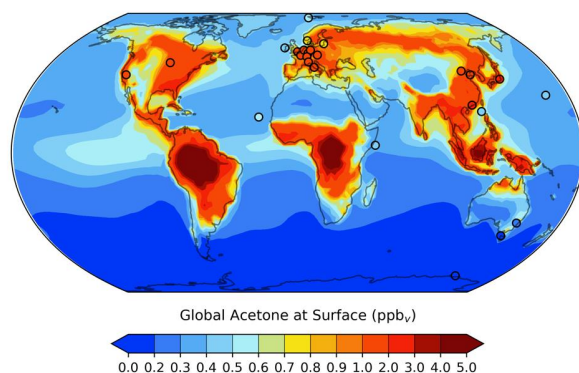
604



605

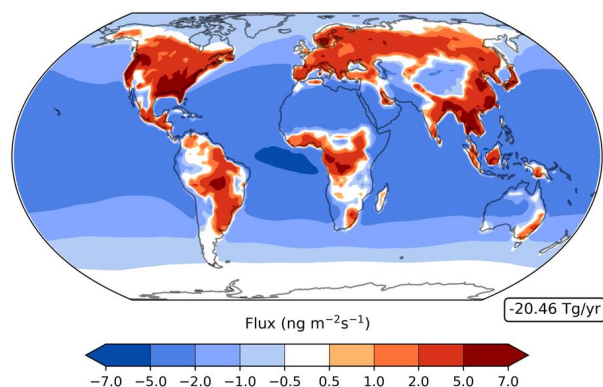
606 **Figure 2.** Total atmospheric burden, fluxes, and lifetimes of acetone from the literature (shown in boxes and whiskers with outliers
 607 as open circles), and values from GISS ModelE2.1 (shown in solid circles). The number of models used to create each box and
 608 whisker plot are labelled. Note that deposition and ocean net fluxes were multiplied by 2 and biomass burning and anthropogenic
 609 emissions were multiplied by 10 for a better visualization of the distribution.

610



611

612 **Figure 3.** GISS ModelE2.1 spatial distribution of annual mean acetone at surface for the Baseline simulation. Filled circles
 613 represent data from twenty-six field measurements (de Gouw et al., 2004; Dolgorouky et al., 2012; Galbally et al., 2007; Guérette
 614 et al., 2019; Hu et al., 2013; Huang et al., 2020; Langford et al., 2010; Lewis et al., 2005; Li et al., 2019; Read et al., 2012; Schade
 615 & Goldstein, 2006; Singh et al., 2003; Solberg et al., 1996; Warneke & de Gouw, 2001; Yoshino et al., 2012; Yuan et al., 2013).
 616 The root mean squared error and the R^2 value between the Baseline acetone estimations and the field measurements are 0.3494
 617 and 0.8306, respectively. A nonlinear colorbar is used to better differentiate the details in the map.

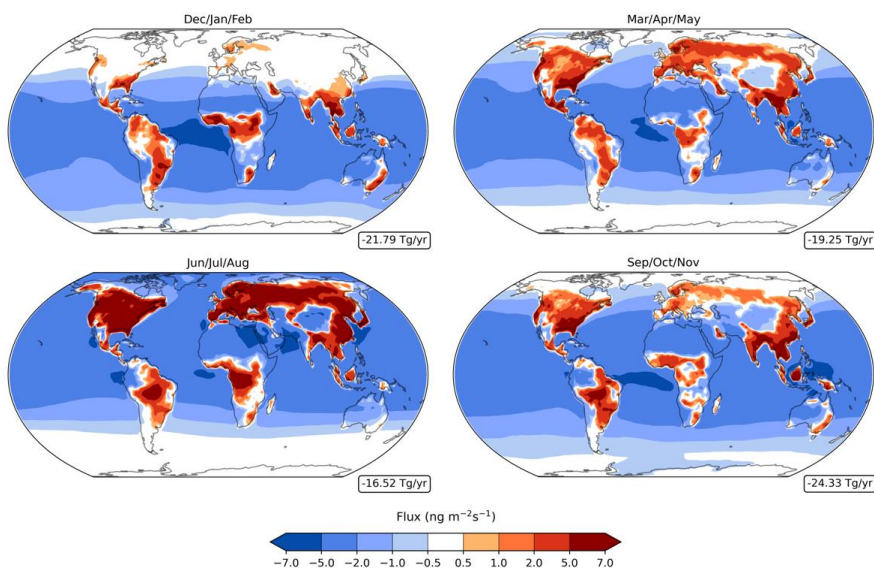


618

619 **Figure 4.** Annual average of acetone net chemistry fluxes (column-integrated) in the Baseline simulation, with red indicating a net
620 source and blue indicating a net sink. A nonlinear colorbar is used to better differentiate the details in the map. The weighted global
621 mean of the net chemistry flux is shown in a box on the lower right.

622

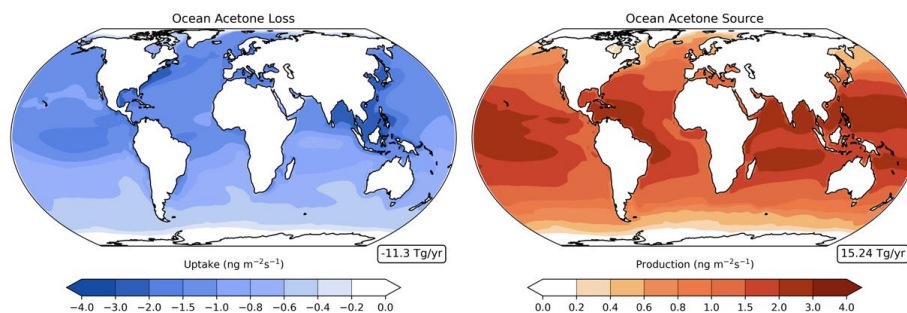
623



624

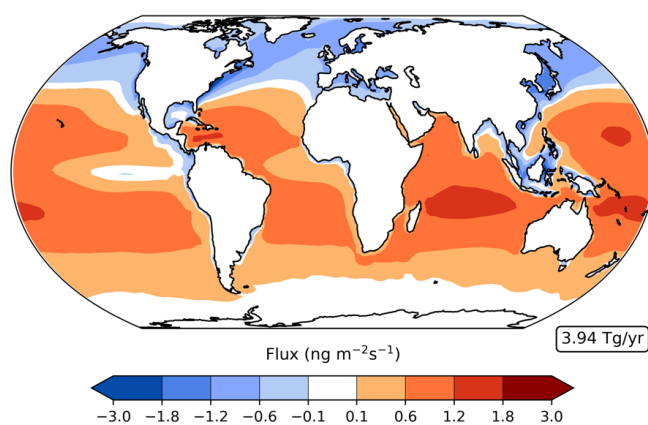
625 **Figure 5.** Acetone net chemistry fluxes (column-integrated) in the Baseline simulation for December-February (top left), March-
626 May (top right), June-August (bottom left), and September-November (bottom right), with red indicating a net source and blue
627 indicating a net sink. Nonlinear colorbars are used to better differentiate the details in the map. The weighted global means of the
628 net chemistry fluxes are shown in boxes on the lower right.

629



630

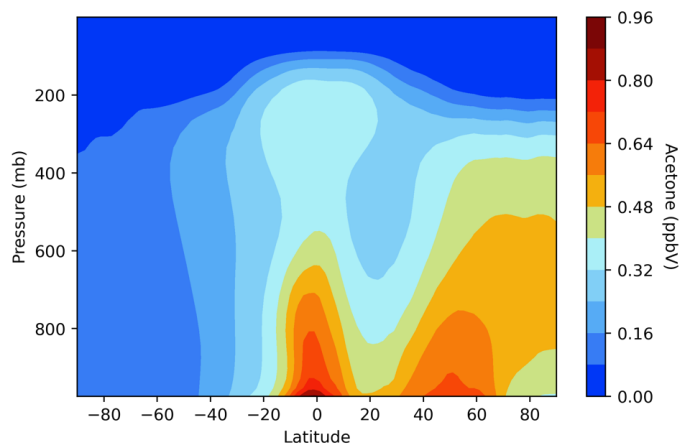
631 **Figure 6.** Annual average of the acetone ocean loss (left) and ocean source (right) in the Baseline simulation. Nonlinear colorbars
632 are used to better differentiate the details in the map. The corresponding weighted global means of the ocean fluxes are shown in
633 boxes on the lower right.



634

635 **Figure 7.** Same as Figure 4, for the ocean bidirectional fluxes.

636



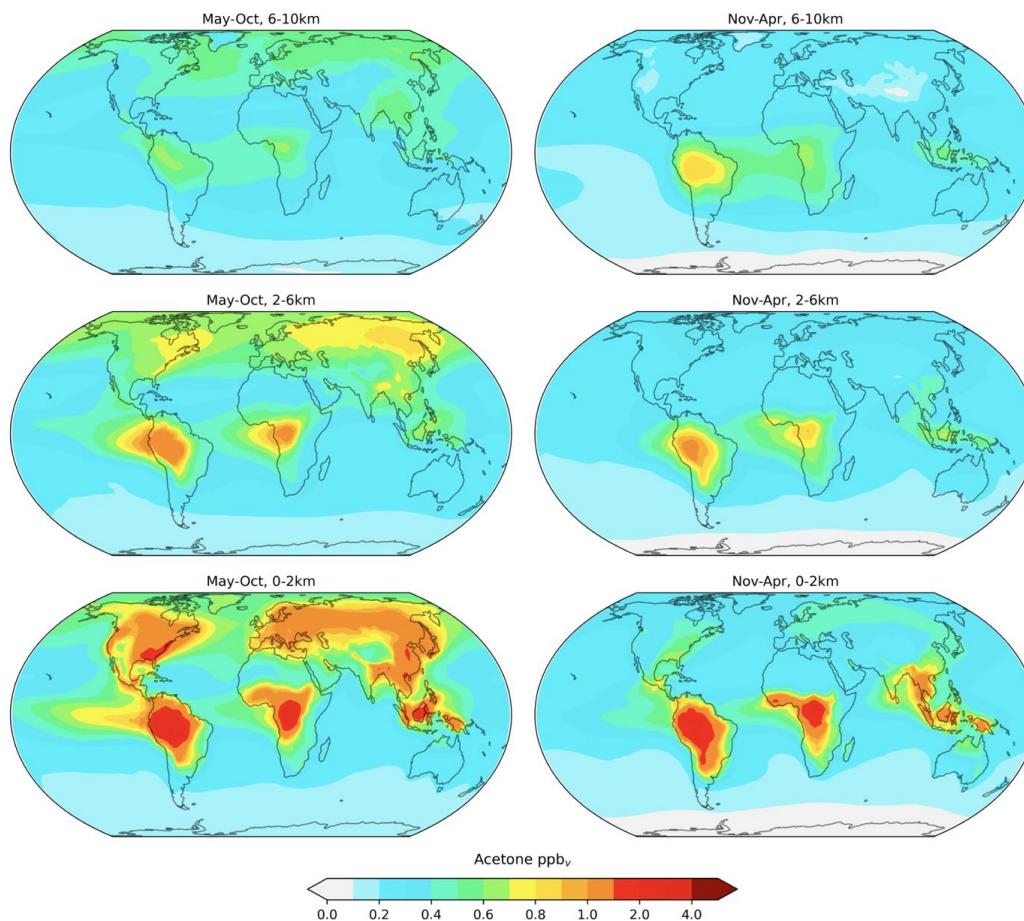
637

638 **Figure 8.** GISS ModelE2.1 vertical distribution of acetone air mixing ratios across latitudes in the Baseline simulation.

639



640



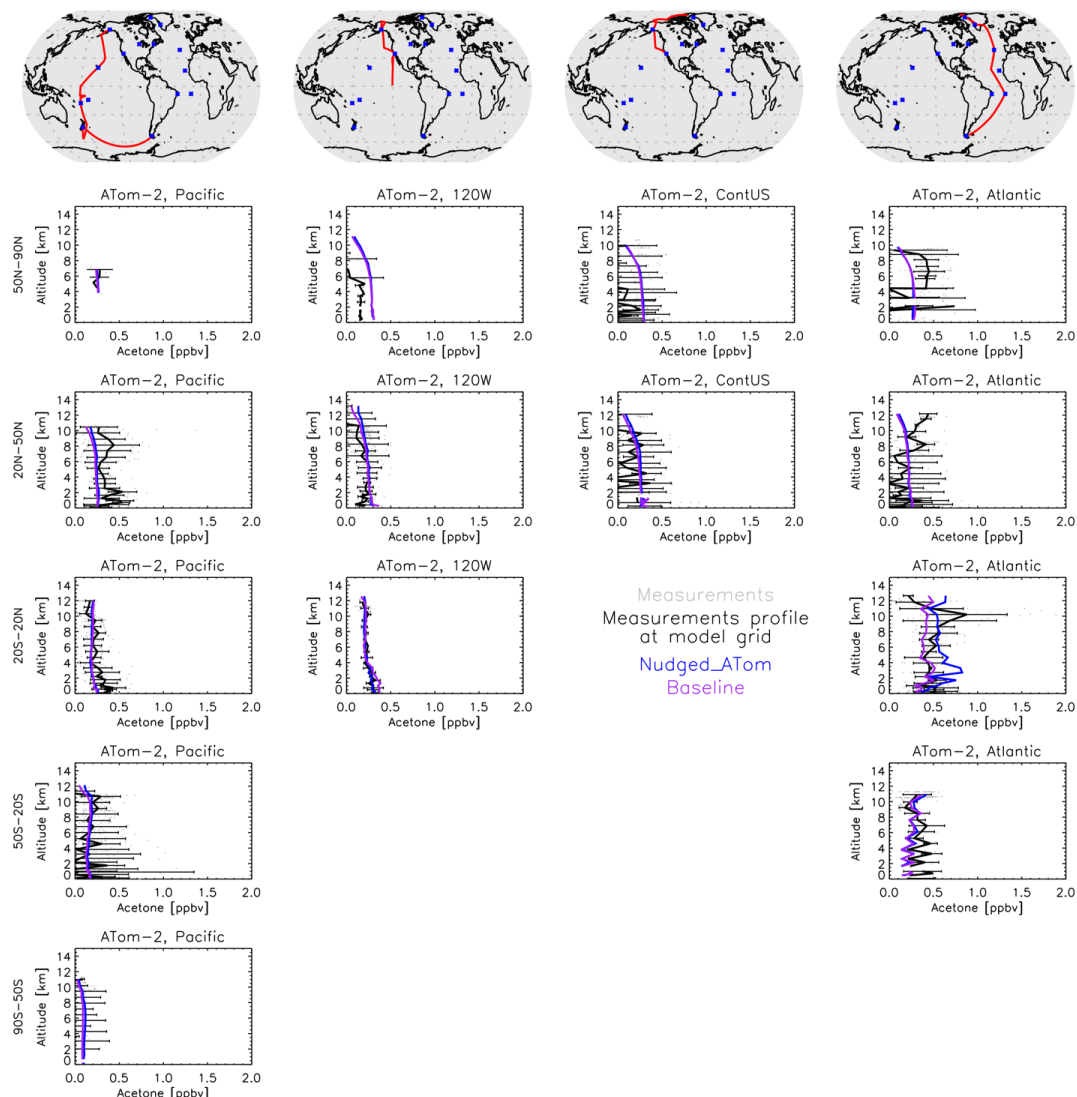
641

642 **Figure 9.** Baseline simulation acetone mixing ratios in the atmosphere at 0-2 km (bottom), 2-6 km (middle), and 6-10 km (top) for

643 the months of May-October (left) and November-April (right). The mixing ratios in the vertical were averaged with an arithmetic

644 mean. The choice of the slices and colors match those in Figure 1 by (Fischer et al., 2012).

645



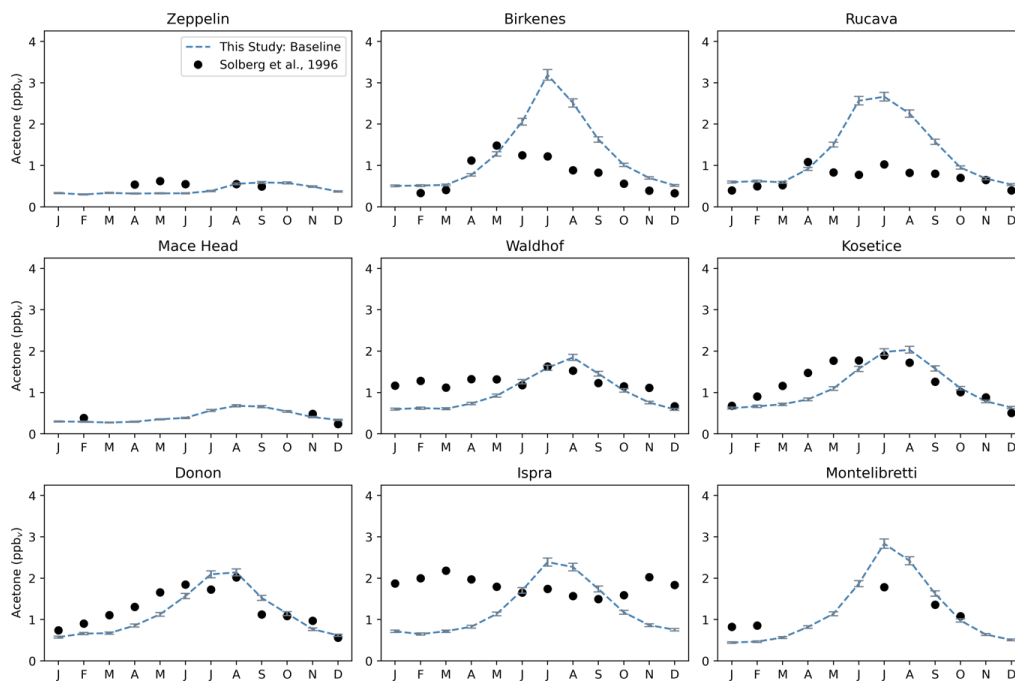
646

647 **Figure 10.** Comparison between the GISS ModelE2.1 simulations (Baseline in purple and Nudged_ATOM in blue) and the ATom-

648 2 field measurements (January-February 2017). Individual data points are shown with grey dots, and their average values are shown

649 in black, with error bars representing the one-sigma range of the averages.

650



651

652

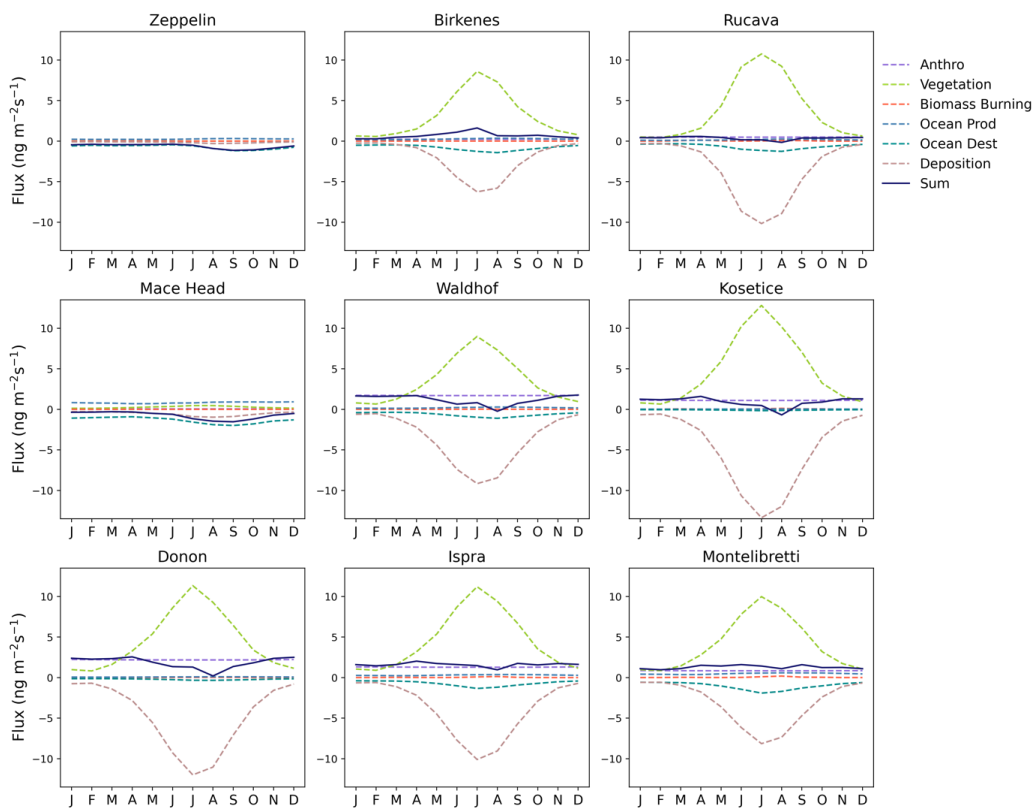
653

654

655

656

Figure 11. Acetone over twelve months at nine European sites, similar to that of Jacob et al. (2002). The modelled estimates of acetone at the surface from the Baseline simulation are shown in blue dashed lines and the grey error bars represent the one-sigma range of the modelled concentrations in the climatological mean of 5 years. Field measurements from Solberg et al., (1996) are shown as solid dots. Root mean squared error between the Baseline simulation and field measurements are (left to right, top to bottom): 0.1968, 0.8714, 0.8724, 0.0914, 0.3907, 0.3430, 0.3160, 0.9454, 0.5454.

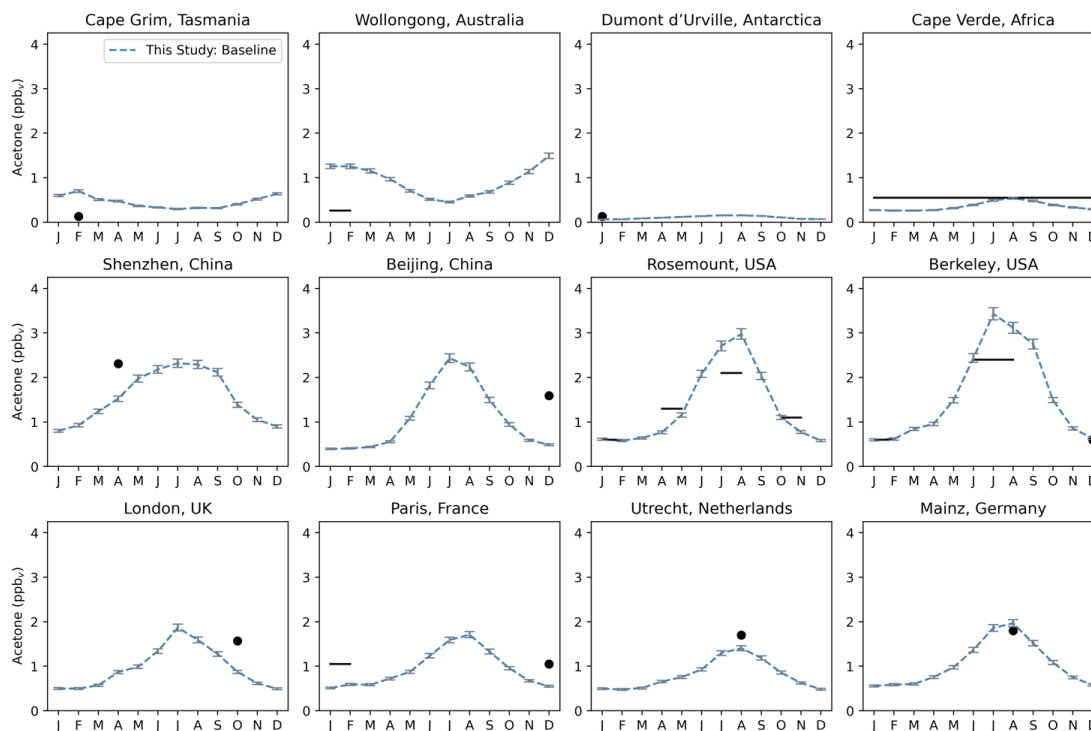


657

658 **Figure 12.** Contribution of acetone sources and sinks in the Baseline simulation over twelve months on the regional level (10° x

659 12.5° grid boxes) at nine European sites.

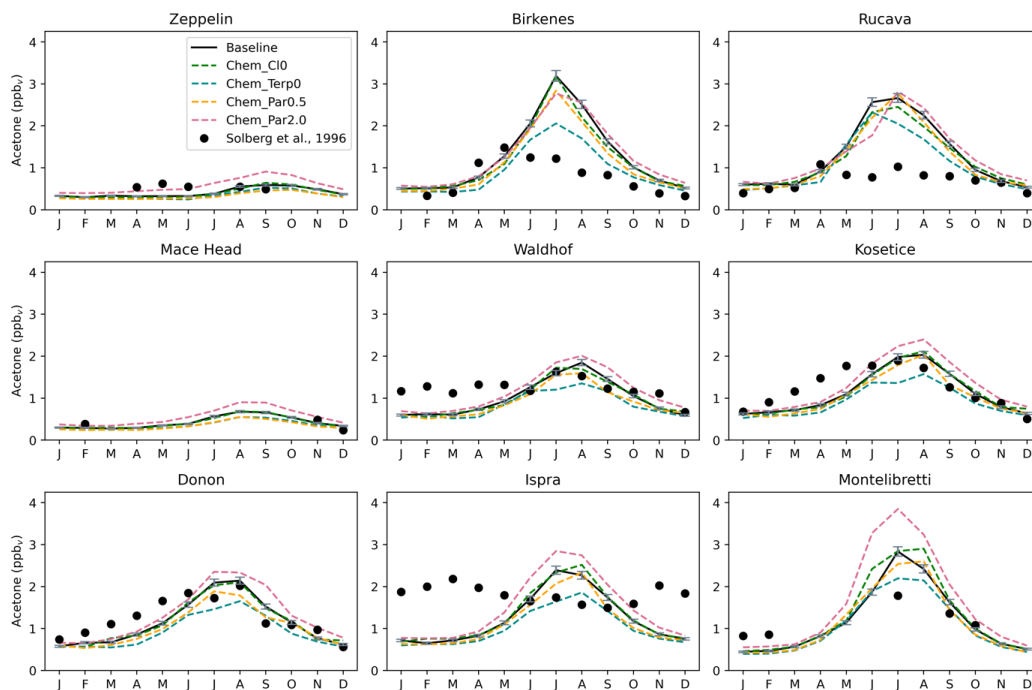
660



661

662 **Figure 13.** A similar plot to Figure 11 for various sites that do not have enough measurements to resolve seasonality (Australia,
663 Antarctica, Africa, Asia, Europe, North America). The modelled estimates are overlaid with monthly (solid circles) or seasonal
664 (solid lines) field measurements, as found in the literature.

665



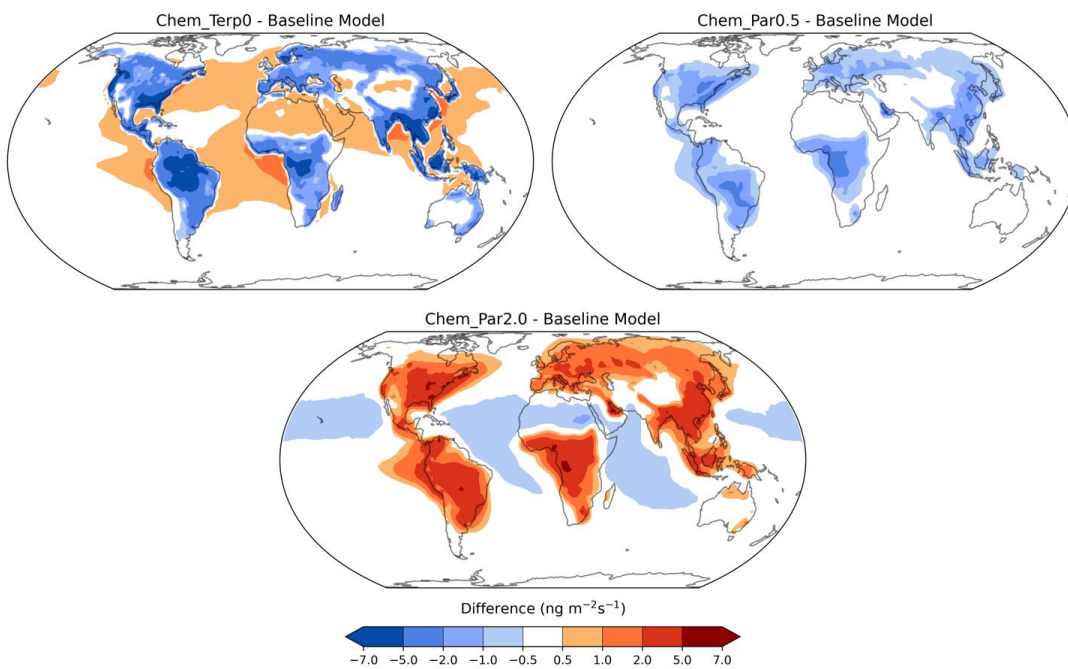
666

667 **Figure 14.** Same as Figure 11 with the chemistry sensitivity studies added. The sensitivity studies include removing the acetone +
668 chlorine reaction (green line), removing the production of acetone from terpenes (blue line), halving the yield of acetone from
669 paraffin (orange line), and doubling the yield of acetone from paraffin (pink line).

670

671

672



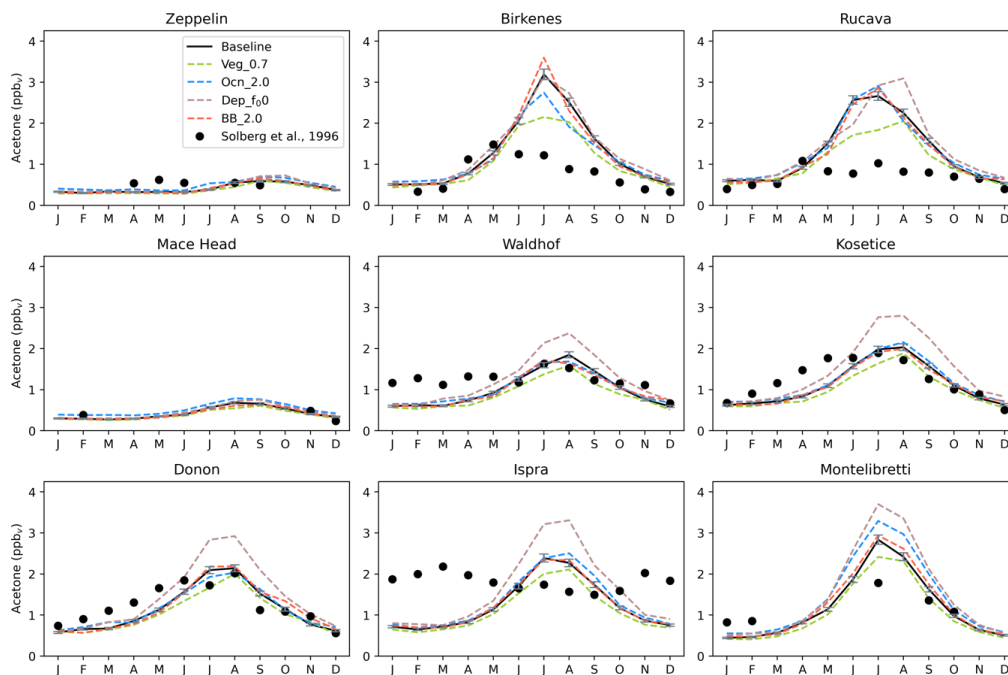
673

674 **Figure 15.** Chemistry sensitivities anomalies from Baseline, with red indicating an increase and blue indicating a decrease of the
675 column-integrated net acetone chemistry flux. Nonlinear colorbars are used to better differentiate the details in the map. The fourth
676 chemistry sensitivity study, Chem_ClO, is omitted, since the changes everywhere are very small, less than $0.4 \text{ ng m}^{-2} \text{ s}^{-1}$.

677

678

679

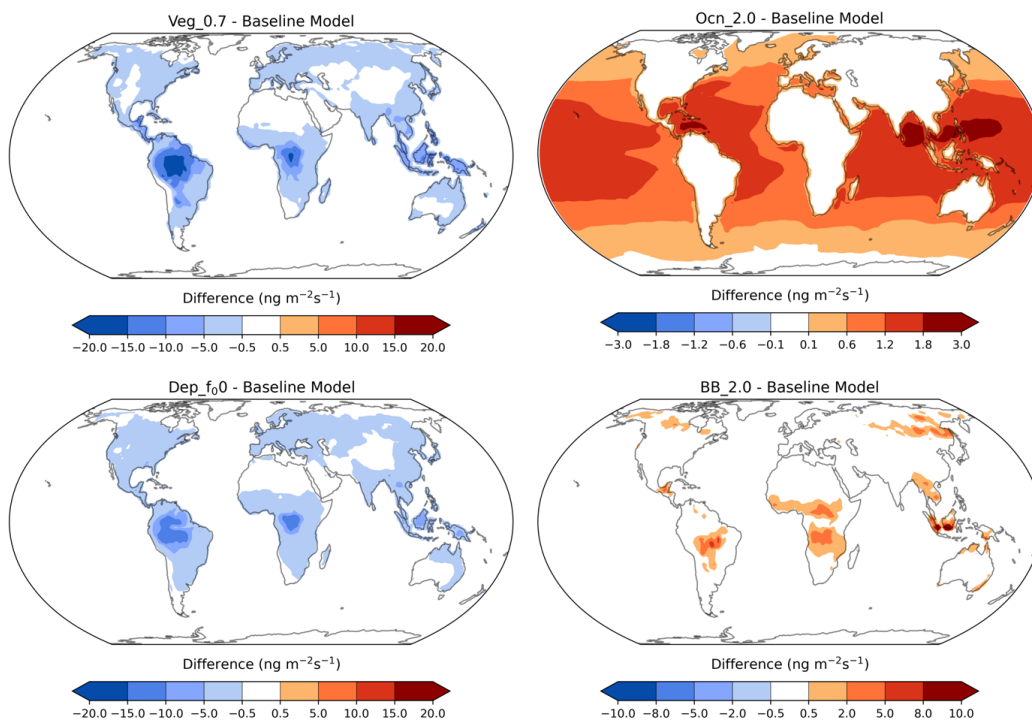


680

681 **Figure 16.** Same as Figure 11 with the terrestrial and oceanic sensitivity studies added. The sensitivity studies include reducing
682 vegetation emissions to 0.7 acetone from MEGAN (light green line), doubling ocean acetone concentration (blue line), changing
683 the reactivity factor for dry deposition (brown line), and doubling biomass burning emissions (orange line).

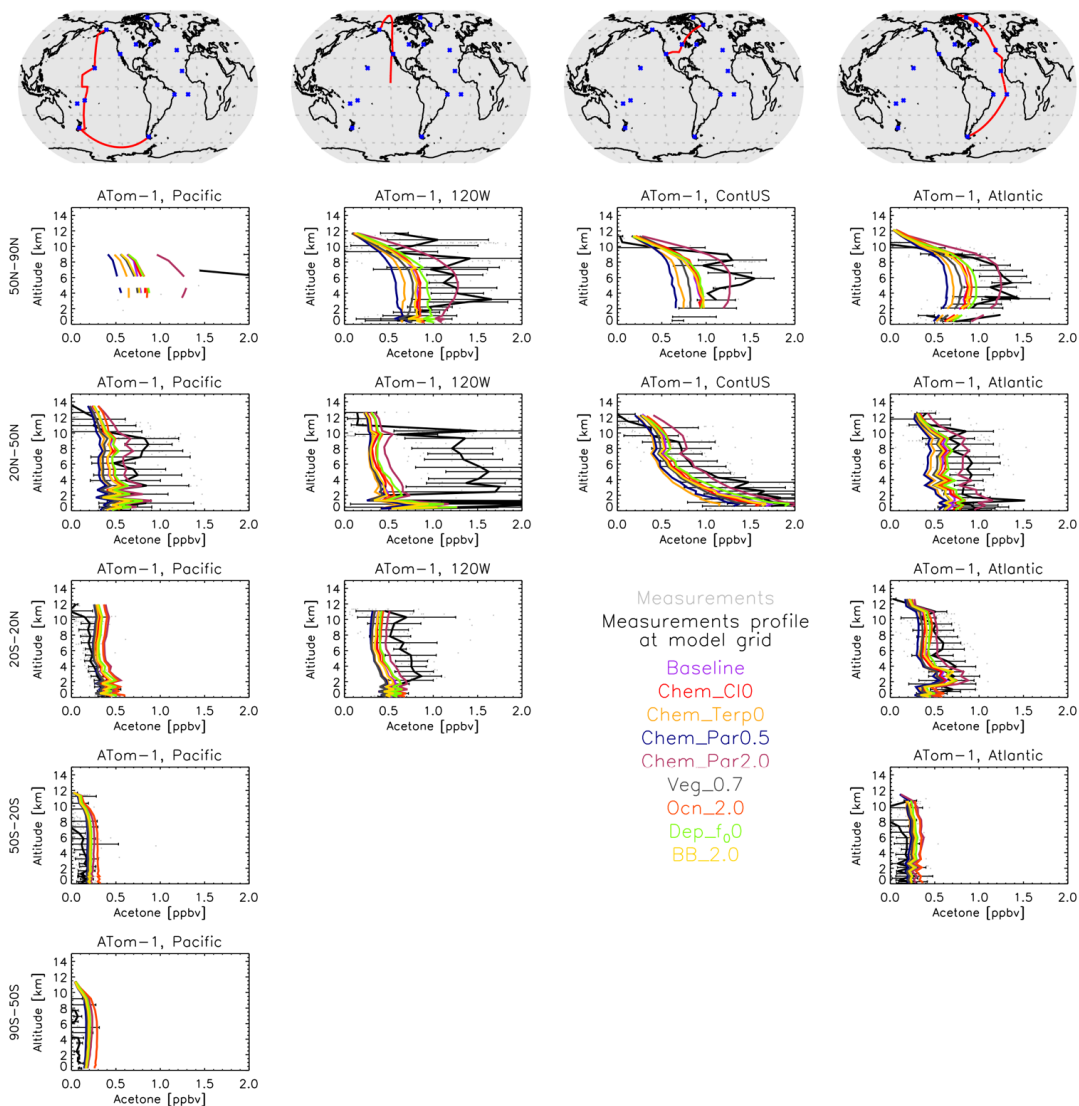
684

685



686

687 **Figure 17.** Acetone anomalies from the Baseline simulation for the vegetation (top left), ocean (top right), dry deposition (bottom
688 left) and biomass burning (bottom right) sensitivities, with red indicating an increase and blue indicating a decrease of the specific
689 flux. Nonlinear colorbars are used to better differentiate the details in the map.



690

691 **Figure 18.** A comparison between the GISS ModelE2.1 sensitivity simulations and the ATom-1 aircraft measurements (July-
 692 August 2016). Note that all sensitivities are to be compared against the Baseline simulation, not the Nudged_ATom one, but as
 693 shown earlier this makes very little difference in the comparison with observations (Figure 10).